Research Performance Progress Report

Project Title:	**Novel Contact Materials for Improved Performance CdTe Solar Cells**
Project Period:	10/01/11 – 12/31/15
Reporting Period:	10/01/11 – 12/31/15
Report:	Final Report
Submission Date:	3/6/16
Recipient:	University of Illinois
Recipient DUNS #:	
Address:	
Website (if available)	
Award Number:	DE-EE0005405
Awarding Agency:	DOE Sunshot F-PACE
Working Partners:	University of Toledo, Old Dominion University
Cost-Sharing Partners:	None
Principal Investigator:	Angus Rockett Professor Phone: 217-333-0417 Email: arockett@illinois.edu
Submitted by:	PI
DOE Project Managers:	Marie Mapes, Department of Energy

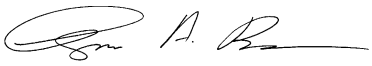

Signature **Date** **3/6/16**

Novel Contact Materials for Improved Performance CdTe Solar Cells

University of Illinois

Angus Rockett

Co-PI's:

University of Toledo

Robert Collins

Old Dominion University

Sylvain Marsillac

This program has explored a number of novel materials for contacts to CdTe solar cells in order to reduce the back contact Schottky barrier to zero and produce an ohmic contact. At the same time, the built-in and open circuit voltages in the device have been increased. CdTe cells in the substrate configuration have been developed to explore high temperature back contact processes that otherwise would modify the CdTe solar cells. All these results have increased the performance of our baseline results and have attracted the participation of industry in evaluating the new back contacts.

1. Project Overview

a. Background

The University of Illinois (UI), the University of Toledo (UT), and Old Dominion University (ODU) are research-oriented universities with research groups having long experience with photovoltaic materials and devices. All three have extensive materials fabrication and characterization facilities, although the UI specializes in characterization while ODU and UT have programs more focused on materials and device fabrication. The UT group has assisted in the development of low cost process technologies applied in CdTe solar cell manufacturing worldwide, notably with First Solar. The UI group has developed a large body of scientific background on Cu-chalocopyrite materials and devices as well as device simulation tools, and has worked across the solar cell community to transfer the knowledge to practice optimizing the processes of individual commercial groups. The ODU group grew out of both the UT and University of Delaware research programs and has a history of cutting edge research on Cu chalcopyrite materials. The UI and ODU groups use similar sputtering-based deposition methods, which complement the UT processing techniques. The UI group specializes in microstructural, microchemical, and optoelectronic characterizations while the UT and ODU groups are leaders in application of ellipsometry for both process control and materials analysis. Collectively the project PI's have more than 60 years of experience in thin film polycrystalline photovoltaics and collaborate with all of the leading manufacturers in the US.

The project outcomes in overview are described as follows. UT has produced both complete baseline superstrate CdTe devices for comparison and test CdTe superstrate devices that lack back contacts. The UT, UI, and ODU groups have deposited novel back contacts on these and have studied the resulting devices, concentrating on selenide, oxide, and nitride materials (UI) and sulfide and oxide materials (ODU). The UT group has also fabricated back contacts from materials that comprise their unique specializations, including thin film Si:H and iron pyrite (FeS_2). All three groups participated in characterization of the resulting structures.

b. Objectives

This project has led to the development and demonstration of devices using novel back contact materials for CdTe solar cells in both superstrate and substrate configurations. In some cases enhanced built-in and open-circuit voltages have been established. The devices have, as a consequence, exceeded the existing baseline performance. We expect that this successful demonstration of an improved contact material can be directly transferred to manufacturers. For contacts of sufficient stability, a completely new range of device geometries will become available based on wider gap heterojunction partner materials. Because much of the planned research described here requires demonstration not only of viable contacts to CdTe solar cells but also the stability of those contacts, a testing protocol is needed. The University of Toledo Center for Photovoltaics Innovation and Commercialization (PVIC) maintains capabilities for

evaluating the stability of contacts to CdTe using various test conditions. For the highest performance back contacts stability of the performance parameters has been evaluated under various operations conditions and environments.

2. Technical Work Plan

Phase I – First 18 months

Phase I results can be summarized in surveys of results in three broad categories of new candidate materials as contacts to CdTe photovoltaics: transition metal nitrides, ternary chalcopyrite semiconductors, and thin film silicon semiconductors. In the case of the semiconductors, demonstration of very high dopability was a key component of the project. All classes of materials were checked for stability with respect to CdTe device layers to determine the potential suitability for substrate-geometry applications.

Task #1 – *Demonstration of heavily p-type contact materials*

I.1.0: We synthesized and characterized wide gap chalcopyrite and thin film silicon compounds and tested whether or not they are suitable for back contacts to CdTe. The focus of doping studies on chalcopyrites was on more common compounds ($CuInSe_2$ and $CuGaSe_2$) This task consists of 2 subtasks.

I.1.1 Subtask 1: Deposition and characterization of wide-gap chalcopyrite and thin silicon back contact materials.

(a) Activities at University of Illinois in Doping of Chalcopyrite Materials

$CuInSe_2$, $Cu(In_{0.7}Ga_{0.3})Se_2$, and $AgInSe_2$ films were grown using a hybrid sputtering and evaporation technique. The base pressure of the deposition system is typically ~$7x10^{-4}$ Pa. Metallic Cu, Ag, or (Cu-Ga) and In targets were dc magnetron sputtered independently in a 0.27 Pa sputtering gas consisting of a controlled mixture of ultra-high purity (99.99% purity) N_2 and Ar. Se was supplied from an effusion cell at the same time. The relative gas pressures were not monitored during growth. The partial pressure for N_2 was established by adjusting a needle valve with the pressure measured using a capacitance manometer. The Ar flow was then adjusted to bring the total pressure to the desired total sputtering gas pressure by adjustment of a second needle valve. For $Cu(InGa)Se_2$ (CIGS) the Cu target was replaced with a Cu-Ga alloy target, resulting in films with a Ga/In+Ga ratio of ~0.3. The sputtering currents on the Cu and In targets were controlled to achieve the desired film stoichiometry. The Se cell temperature set-point was initially adjusted to 520°C to reach the desired temperature quickly, then reduced to 320°C for the duration of the growth, resulting in a Se deposition rate of ~40 nm/min. The sputtering sources were separated from the substrate by 25 cm, while the evaporation cell is 18 cm from the substrate. At the operating pressure both the sputtered species and the Se are expected to undergo a number of scattering events in the gas phase, thermalizing any high energy sputtered particles, before reaching the substrate. The substrate was clipped to a sealed resistive

heater. Temperature was measured both with a thermocouple attached to the heater block and using a pyrometer to measure the substrate temperature directly.

Three substrates were used for the growth of films. Polished (100) oriented GaAs for growth of epitaxial CIS films. Epitaxial films are of interest to this study because they eliminate the complicating effect of grain boundaries and generally exhibit much higher carrier mobilities than polycrystals. Films grown on soda lime glass substrates were studied because soda lime glass has a similar thermal expansion coefficient to that of CIS, is used in devices, and supplies Na_2O to the growing film. The Na_2O is converted to Na_2Se in the Se flux on the substrate surface or in the CIS layer due to the high activity of Se. Finally, single crystal Si wafers with a native oxide, were used to grow polycrystals at elevated temperatures (above the soda-lime softening temperature) and without Na.

For doping of the CIS, group V elements were introduced during growth using two different methods. N_2 was added to the sputtering gas, keeping the overall pressure constant. An effusion cell was used to supply Sb while sputtering was conducted with Ar gas. In films grown on GaAs, As diffused into and through the film. In almost all cases no As was detectable in the resulting CIS epitaxial films by secondary ion mass spectrometry (SIMS). Group V elements were also implanted into undoped films using ion implantation. Five films grown without any group V dopants, and slightly Cu poor compositions, were implanted with N^+ at an energy of 400 keV and a dose of $5x10^{15}$ cm^{-2}. This led to a projected range of 500 nm, in 700 nm thick films and a peak concentration of N expected to be 10^{20} cm^{-3} (0.2 atomic percent). This energy deposits the majority of the dopant atoms in the 0.75 micron thick films.

Film stoichiometry was determined through energy-dispersive X-ray spectroscopy (EDS) analysis. Films were slightly Se rich, with an average Se content of 52%, while Cu content was kept low, on average ~23%. Hot point probe measurements indicated that the films were p-type. Sheet resistance was measured with a four-point probe, and then converted to resistivity using the film thicknesses.

(b) Activities at University of Toledo in Doping of Chalcopyrite Materials

The $CuInSe_2$:N (CIS:N) deposition process applied at University of Toledo (UT) involves sputtering of copper and indium in Ar/N_2 along with simultaneous evaporation of selenium in a sputtering/evaporation hybrid deposition system. Prior to the application of these layers in actual solar cell devices, a series of experiments was performed to determine the deposition parameter baseline that gives the stoichiometric CIS phase. For this purpose, films were deposited on soda lime glass at a substrate temperature of 500 °C using various combinations of power levels applied to the Cu and In targets. Se was evaporated at a source temperature of 320 °C and the evaporation rate was ~ 13 Å/s. Table 1 lists the deposition parameter values for co-sputtering of Cu and In targets and thermal evaporation of Se in the UT hybrid deposition system. For the deposition of the CIS:N layer in the solar cell device, however, the device cannot be heated to

500 °C. Upon heating to such a high temperature, the CdTe evaporates in a low pressure environment (2.5 mTorr of Ar/N_2). Thus, during the CIS:N layer deposition on CdS/CdTe devices, the deposition temperature was reduced by necessity to 375 °C, a temperature identified by performing real time SE and monitoring the thickness loss of the CdTe.

Table 1. Listed in the table are the parameters for CIS and CIS:N depositions on borosilicate glass in the UT hybrid deposition chamber. For application of these layers in the device structure, however, the substrate temperature was by necessity reduced from 500 °C to 375 °C to prevent the evaporation of underlying CdTe material which occurs at the high temperature and low ambient pressure of the hybrid process.

Layer deposited on Borosilicate glass	**Deposition parameters**									
	Processing pressure (mTorr)	Ar flow rate (sccm)	N_2 flow rate (sccm)	Cu target power (W)	In target power (W)	Se evaporation rate (Å/s)	Substrate temperature (°C)	Se evaporation temperature (°C)	Deposition time (min)	Targeted thickness (nm)
CIS	2.5	30	0	36	40	13	500	350	10	100
CIS:N	2.5	15	15	36	40	13	500	350	10	100

In some cases, CIS:N layers were deposited in a two-step process that involves the deposition of first one fourth of the layer thickness at 375 °C and the remaining three-fourths at 450 °C. The devices were finally completed with 1 μm Mo deposited by sputtering using a metal mask to define the area.

CIS deposited by a wet process (spray pyrolysis deposition) was also applied as a back contact layer in both sputtered (best 13.5%) and close-space sublimated (CSS) CdTe devices (best 16%) in the superstrate configuration. These devices were also completed by the deposition of 1 μm Mo by sputtering to define the device area. Figure 1 shows schematic of the completed solar cell device structure in standard and novel back contact configurations. The results of material characterization and device performance will be discussed in a later section of the report. To prepare CIS thin films in the wet process, spray pyrolysis employed a hydrazine-based solution. The precursor solution used for the spray consisted of 1 ml 0.5 M Cu_2S in hydrazine, 1.2 ml 0.25 M In_2Se_3 in hydrazine, 0.8 ml 2 M Se in hydrazine, and 22 ml DI-water. To deposit the films, the precursor solution was delivered to an ultrasonic nozzle (Sonotek, Impact Head) at a flow rate of

0.2 ml/min by a modified HPLC pump where it was atomized and transported to a substrate on a heated translation stage at 350 °C using a directed N_2 flow. The temperature was selected to ensure applicability of the method for back contact fabrication in CdTe solar cells. The 100 nm thick CIS film was deposited in 15 min and then annealed on the stage for 30 min at the deposition temperature of 350 °C, which converts the precursors to the chalcopyrite CIS phase.

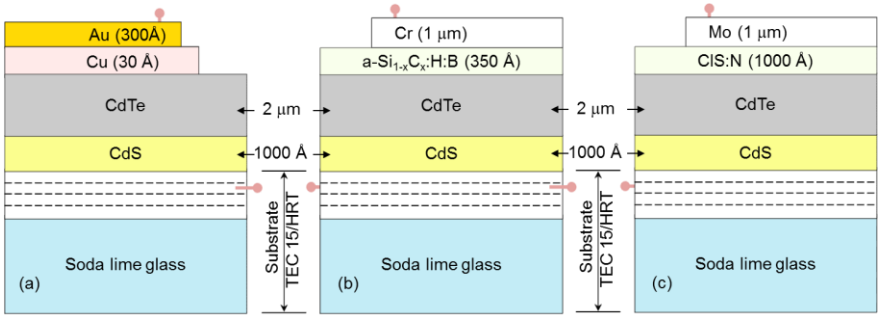

Figure 1. The schematic of device configuration is shown for (a) the standard CdTe solar cell with a Cu/Au back contact, (b) a CdTe cell with a novel *p*-type a-$Si_{1-x}C_x$:H:B back contact and Cr as the final metal contact to define the cell area and (c) a CdTe cell with a novel *p*-type CIS:N back contact and Mo as the final metal contact to define the cell area. The layers beneath the CdS are the coatings of the TEC-15/HRT superstrate.

(c) Activities at University of Toledo in Thin Film Silicon Deposition

The a-$Si_{1-x}C_x$:H *p*-layers incorporated into the CdTe solar cells were prepared by plasma enhanced chemical vapor deposition (PECVD). The deposition parameters were selected for optimum a-Si:H based solar cell performance in the *p-i-n* configuration, including the following: substrate temperature, 200 °C; rf power density, 0.01 W/cm^2; total pressure, 0.4 Torr; SiH_4 flow rate, 13 sccm; (5 vol.% B_2H_6 in H_2) flow rate, 1 sccm; and CH_4 flow rate, 8 sccm. The deposition time was 150 seconds for an intended a-$Si_{1-x}C_x$:H *p*-layer thickness of 350 Å. Films prepared under similar conditions to a thickness of 3000 Å exhibited bandgaps of ~ 1.90 eV from spectroscopic ellipsometry by the Cody method (or ~ 1.94 eV from transmission and reflection spectroscopy by the Tauc method) (Ferlauto *et al*., 2002). The conductivity of such films was in the range of (1-2) x 10^{-5} $(\Omega\,cm)^{-1}$. The device was completed by sputter deposition of Cr as the final metal contact that serves to define the cell area. The sputter deposition parameters for Cr include: substrate temperature, room temperature; rf power density, 0.92 W/cm^2; Ar sputtering pressure, 5 mTorr; and Ar flow, 10 sccm. Cr was deposited for 40 min with a targeted thickness of 1 µm. The layer stack for this device structure is shown in Figure 1 (b). The performance parameters of the devices with standard and novel back contacts were measured under 1.5 AM illumination. To study the degradation of the devices with time, the cells have been measured at

various intervals under the same illumination over a two year period. Table 2 lists the details of *p*-layer and Cr layer depositions.

In separate experiments designed to understand the stability issues encountered, the $CdCl_2$-treated CdTe cell structure was exposed to a H_2 plasma for 15 seconds before completion with the standard Cu/Au back contact. The conditions for H_2 plasma exposure included heating the sample to 200 °C and were similar to those of a-$Si_{1-x}C_x$:H:B deposition. The 22 sccm flow of hydride gases used in a-$Si_{1-x}C_x$:H:B deposition was replaced by the same flow of H_2, but an elevated total pressure of 1 Torr was used for the H_2 relative to the hydrides to ensure stable plasma ignition. Each of the samples incorporated thirty working dot cells having an area of 0.125 cm^2 each. The performance of the H_2 plasma exposed solar cells has been compared with a standard device from the same run, and in these experiments individual cells were measured at various intervals over a 2 month period.

Table 2. Deposition conditions listed in the table are relevant for the fabrication of the a-$Si_{1-x}C_x$:H *p*-layer and the Cr layer by PECVD and sputtering, respectively, used as a novel back contact combination in CdTe solar cells. The deposition parameters for the a-$Si_{1-x}C_x$:H *p*-layer optimize a-Si:H based solar cell performance in the *p-i-n* configuration.

Layer Type	**Dep. Pressure (mTorr)**	**RF Plasma Power (W/cm^2)**	**Substrate Temp. (°C)**	**Time (s)**	**Gas Flows (sccm)**	**Intended thickness (Å)**
p-layer	400	0.01	200	150	[SiH_4] = 13 [5 vol.% B_2H_6 in H_2] = 1 [CH_4] = 8	350
Cr	5	0.92	RT	2400	[Ar] = 10	10000

I.1.2 Subtask 2: Demonstration of high level p-type doping of chalcopyrite materials.

The goal of this portion of the work was to demonstrate controlled high-level p-type doping of $CuInSe_2$ (CIS) and related materials. Controlled addition of N and Sb to the deposited materials was carried out and the effect on optoelectronic properties was determined. The project studied a range of materials but focused primarily on CIS as no major differences in behavior of the other Cu or Ag chalcopyrite materials was observed. Successful high levels of conductivity in the films was demonstrated, although the electrical activity of the N atoms in the CIS was low overall. Although high levels of N were incorporated, no significant changes in film structure were observed.

(a) Activities at University of Illinois in Doping of Chalcopyrite Materials

Typical morphologies of films grown on each of the three substrates investigated are shown in Figure 2. All polycrystalline films showed a dense columnar microstructure. The films on Si

show a larger grain size compared to those on soda-lime glass. Films on GaAs were found to be epitaxial with a tendency to facet to (112) planes, similar to what has been observed previously. Successful epitaxial growth was confirmed by XRD. Secondary electron microscopy was used to measure film thickness via fracture cross sections, which showed that growth rates were consistent for all N_2 partial pressures studied including pure N_2. The films were ~0.75 microns thick.

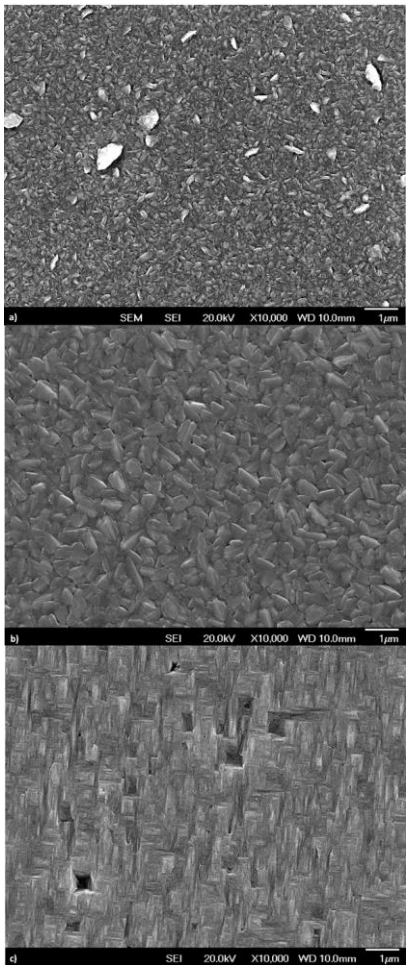

Figure 2: plan view SEM images of CIS films grown on a) soda lime glass, b) Si (111), and c) GaAs (100).

Adding N_2 to the process changed the sputtering rates. For N_2 fractions in the sputtering gas over 70% the films showed an increase in Cu content and a decrease in Se content. For example, for N_2 > 70% the Cu/In ratio increased from ~0.75±0.05 to 1.15±0.05. This was attributed to nitridation of the In target, resulting in a reduction in its sputtering rate. Presputtering the In target before deposition for two minutes increased the In content substantially in support of this interpretation. The decrease in Se is consistent with the change in Cu/In ratio as typical for the pseudobinary phase diagram for Cu_2Se and In_2Se_3.

For growth on GaAs substrates zero to 10% N_2 in the sputtering gas, films were fully epitaxial as shown by XRD (Figure 3). Higher N_2 concentrations led to some evidence of other orientations of CIS.

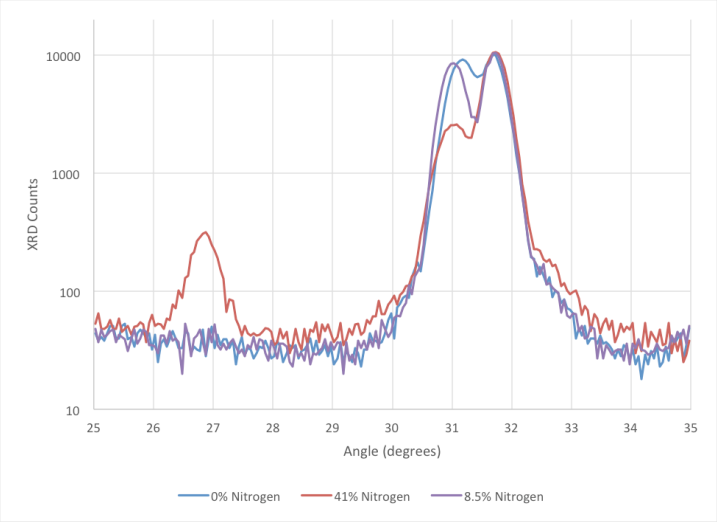

Figure 3: XRD scans for films grown on GaAs (100). The peak at 31.675° is due to the GaAs (001) planes. The peak to the left at ~30.975° is due to GaAs. The CIS film peak is located at 31.125° for the film sputtered in pure Ar. There is probably not a true peak shift as N_2 is added. Rather the peak width is probably changing, resulting in more overlap. For higher N_2 partial pressures (eg: 41% in the sputtering gas) a secondary peak due to grains of different orientations begins to appear, indicating a partial transformation to polycrystalline material.

For polycrystalline films grown on soda-lime glass the films exhibited a change in texture at high N_2 partial pressures. For N_2 below ~40% in the gas phase the films were randomly oriented. Above this composition the (112) peak intensity increased rapidly resulting in films with N_2 greater than ~50% in the gas phase having 20-80x greater (112) peak height relative to random orientation. By contrast, films on oxidized Si showed ~10x more (112) orientation intensity than for films on soda lime glass for those deposited with either pure Ar or pure N_2, while other

intermediate N_2 fractions tested showed only random texture. No second phases were observed in the polycrystalline films by XRD.

Film compositions were determined by energy dispersive x-ray fluorescence spectroscopy (EDS) in a Hitachi 7000 SEM with a windowless EDS detector (necessary to detect light elements). Quantitative analysis was carried out and N contents ranging from undetectable to ~6 atomic percent (at.%) were measured as the N_2 partial pressure was increased in the deposition system during growth. At the same time a decrease in Se content from ~52 to ~46 at.% was observed as shown in Figure 4. While there is considerable scatter in the EDS data (estimated as ±1 at.%), there is a consistent trend with a unity slope, suggesting a direct substitution of N for Se. This would have been expected to produce heavy p-type doping of the material. While high doping levels were achieved (see below), the electrical activity of the incorporated N atoms was low. This is unexpected for a direct substitution of N (group V) for Se (group VI) unless there was a change in lattice structure or stoichiometry otherwise. We do observe an increase in Cu content relative to In as N_2 was added to the process gas. However, this generally goes the wrong direction for compensating an acceptor state. We do not observe evidence of any second phase and there is no evidence of an amorphous phase in the broad background spectrum in the CIS. Indeed, the background XRD intensity for films grow on Si seems to decrease at higher N_2 fractions in the gas phase, possibly suggesting better organization of the deposited material.

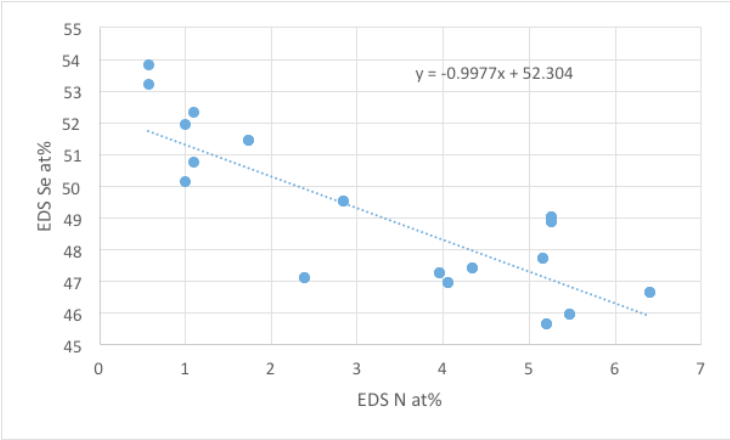

Figure 4: EDS Se composition in the CIS films deposited for this study as a function of EDS N concentration in the film (both in atomic percent). The slope of the dashed line is unity, suggesting a 1:1 substitution of N for Se.

N incorporation into the films was also studied by secondary ion mass spectrometry (SIMS) with a primary beam of Cs^+ ions and detecting Cu and In using positive secondary ions or $(Cs+N)^-$ or Se^- ions for the electronegative ions. SIMS is relatively insensitive to N ions of any polarity. This measurement produced less reliable results due to the difficulty of quantifying SIMS data

but showed an increase in N in the films for N_2 fraction in the gas phase over ~30%. The incorporated N in the films was found to increase roughly exponentially with increasing N_2 in the process gas.

Four point probe measurements were used to determine film resistivities resulting from N addition. Spring-loaded blunt W probes with a 1 mm spacing were used to contact the samples. Film thicknesses used to convert sheet resistance to resistivity were obtained by SEM fracture cross-sectional images. Resistivities on soda-lime glass and Si substrates were very similar at low N_2 levels, while for higher N_2 fractions in the sputtering gas the resistivity of films on soda lime glass continued to decrease while the films on Si remained roughly constant in resistivity (Figure 5). We note that soda-lime glass is well known to supply Na to the films during growth and to improve devices, generally by reducing compensation and increasing effective p-type doping level. This may account for the greater dopability of films grown on soda-lime glass. The resistivity decreased exponentially or faster (Figure 5) as N_2 partial pressure increased, indicating an increasing rate of incorporation of N in electrically-active sites as a function of N_2 partial pressure, in agreement with the SIMS data.

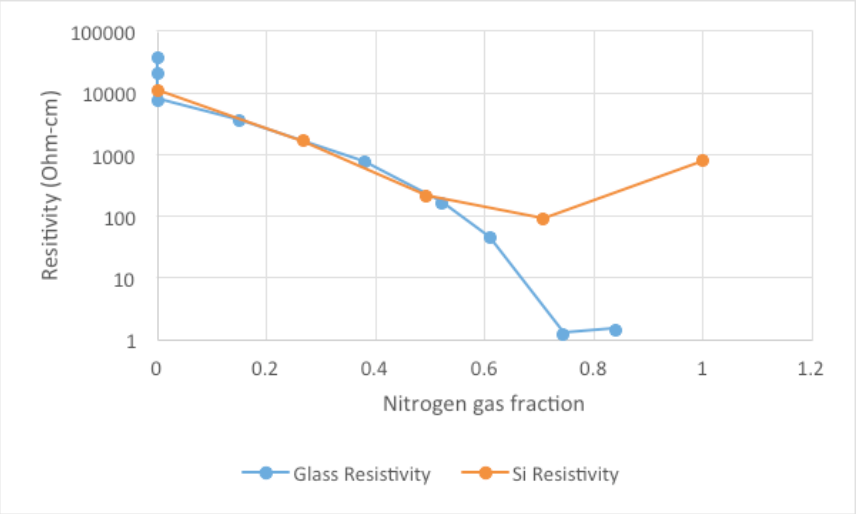

Figure 5: film resistivity determined by four point probe as a function of N_2 gas fraction in the sputtering gas.

The resistivity was also checked by implantation of N into high resistivity CIS films. Five films were grown without added N_2. All showed high sheet resistances between 250 and 6500 Ω-cm as deposited. After implantation the resistivities were reduced by a factor of ~2000 to between 0.1 and 1 Ω-cm. However, these films were not annealed following implantation so this may reflect a damaged film rather than a true reduction in resistivity.

(b) Activities at University of Toledo in N-Doping of Chalcopyrite Materials

This section includes results obtained at UT on the optical and electrical characterization of the undoped and nitrogen doped CIS layers deposited at UT by the hybrid process on borosilicate glass. Figure 6 shows the SEM micrographs of the CIS:N layer at two different magnifications. The deposition process yielded a granular structure with average grain size of ~ 300 nm. XRD performed on this sample indicated the stoichiometric $CuInSe_2$ phase. Energy dispersive X-ray spectroscopy (EDS) was performed on the sample to determine the elemental compositions and yielded atomic percentages of Cu, In and Se of 26 at.%, 22 at.%, and 52 at.%, respectively, for CIS:N deposited on borosilicate glass, indicating a nearly stoichiometric $CuInSe_2$ phase of the layer as observed by XRD. The presence of the atomic nitrogen (dopant) could not be detected by EDS.

Infrared spectroscopic ellipsometry (IR-SE) data spanning the photon energy range of 0.05 eV to 0.8 eV were acquired and analyzed. Table 3 presents the free carrier parameters as determined from IR-SE data analysis. From ex-situ IR-SE analysis, the enhanced conductivity of the CIS layer due to nitrogen doping could be detected. The significant reduction in the scattering time upon doping appears to limit the ability of the increased concentration of holes to reduce the resistivity. Figure 7 shows the dielectric functions for doped and undoped CIS layers deposited on borosilicate glass as obtained by IR-SE analysis. This figure clearly indicates larger free carrier absorption in the doped sample in the lower energy region of the spectrum. The short scattering time for CIS:N, however, leads to a long absorption tail as indicated by the imaginary part of the dielectric function ε_2, extending into the near infrared range.

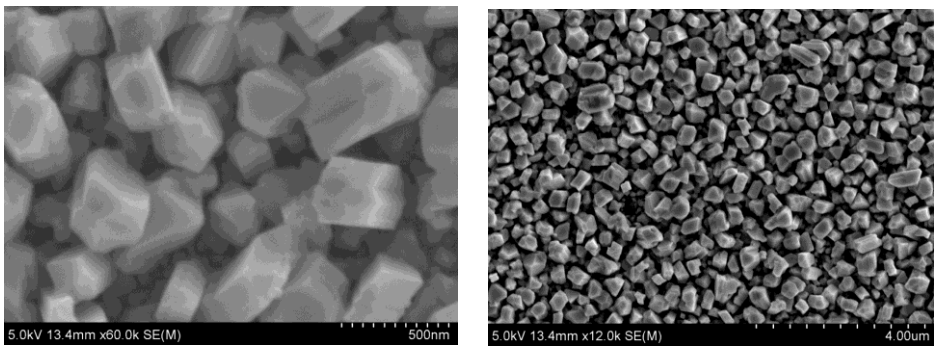

Figure 6. Scanning electron microscopy (SEM) image of CIS:N layer deposited on soda lime glass are shown at two different magnifications. The image shows the granular structure with average grain size of ~ 300 nm. XRD performed on this sample indicated a dominant stoichiometric $CuInSe_2$ phase.

Table 3. Material characteristics for CIS and CIS:N layers deposited on borosilicate glass were determined from infrared spectroscopic ellipsometry (IR-SE) characterization over the spectral range of 0.05 – 0.80 eV. To calculate the carrier concentration and mobility from the IR-SE measurements of the resistivity and scattering time, a hole effective mass of $m_h^* = 0.76\ m_e$ was assumed.

	IRSE Analysis					
Layer	Resistivity (Ω-cm)	Scattering time (fs)	Carrier concentration (cm^{-3})	Mobility (cm^2/Vs)	Layer thickness (nm)	Sheet Resistance (Ω/sq.)
CIS	0.20	1.59	8.4×10^{18}	3.7	180 ± 22	11×10^3
CIS:N	0.061	0.0081	5.5×10^{21}	0.019	150 ± 15	4×10^3

While applying the CIS:N layer in the device in the superstrate configuration, the substrate temperature cannot be raised above the CdTe sublimation temperature, which decreases as the ambient pressure decreases. Thus, it was necessary to maintain the substrate temperature at < 375 °C in CIS deposition on CdTe in order to prevent CdTe evaporation. High temperature CIS layers can be deposited on Mo in the substrate CdTe solar cell configuration and such results will be presented in later in this report.

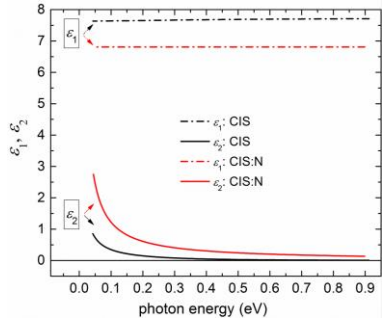

Figure 7. Real and imaginary parts of the dielectric function spectra were obtained by fitting IR-SE measurements results in the mid-infrared to near-infrared range for CIS and CIS:N fabricated by hybrid co-sputtering/evaporation on borosilicate glass.

Task #2 – *Testing of novel contact materials in CdTe solar cells*

I.2.0: We will deposit chalcopyrite materials and conductive nitrides on baseline CdTe solar cells as back contacts and characterize the contact properties by temperature-dependent light and dark current/voltage measurements. From this we will determine the Schottky barrier heights for each of the studied materials. This task consists of four subtasks.

I.2.1 Subtask 1: Deposition of CdTe solar cells

UT will deposit baseline CdTe solar cells for contacts then deposited at UI and ODU. In addition completed devices with conventional back contacts will be produced and characterized at UT for comparison with the novel contact options. Cells to be deposited on SnO_2 coated Pilkington soda-lime glass or ZnO-coated aluminosilicate glass covered with CdS followed by CdTe. The devices then $CdCl_2$-treated following standard UT procedures. For baseline devices structure will then be finished with standard UT back contacts.

(a) Activities at University of Toledo in CdTe Solar Cell Deposition

(i) *Samples Delivered to the Collaborators*

Toward this subtask, P. Koirala, graduate student at UT, fabricated several different CdS/CdTe sample structures for collaborative work with the group at University of Illinois, Urbana-Champaign (UIUC). These samples include completed CdTe devices in the superstrate configuration having efficiencies > 12%, as well as same band gap tandem device structures. These samples with different layer structures were deposited on various substrates designed for microwave impedance microscopy (MIM) studies to be performed at UIUC. This technique has the potential to provide information on the local carrier concentration on the nanoscale and, thus, doping level within the grains and along the grain boundaries.

(ii) *Improving the Baseline Devices and Student Training*

In addition to supplying collections of solar cells to our partner institutions, continuous attempts are being made toward improving the solar cell performance and statistics. An additional goal of this work was to train a new student graduate student, X. Tan, in the full range of capabilities applied in the fabrication, characterization, and optimization of CdTe solar cells at UT. For this task, X. Tan fabricated devices with standard Cu/Au back contacts incorporating oxygenated

cadmium sulfide ($CdS_{1-x}O_x$) window layers deposited by reactive sputtering of a CdS target in an Ar/O_2 environment.

Figure 8 shows the preparation conditions, sample structure, and a photograph of the completed 256 dot cells fabricated under a fixed set of conditions over a 15 cm x 15 cm substrate area. Because the semiconductor layer depositions are not uniform, a range of thicknesses can be deposited in a single run, and this enables simultaneous optimization of the $CdS_{1-x}O_x$ thickness along with the process variables. Figure 9 (left) shows a map of the $CdS_{1-x}O_x$ thickness over the area of the substrate as obtained by through-the-glass spectroscopic ellipsometry on the final device structure fabricated with a $[O_2]/\{[O_2] + [Ar]\}$ ratio of 0.1. These thickness values are spatially correlated with the device performance in Figure 9 (right) for three depositions with different $[O_2]/\{[O_2] + [Ar]\}$ ratios. Optimum performance is obtained for a $[O_2]/\{[O_2] + [Ar]\}$ ratio of 0.1 and a $CdS_{1-x}O_x$ thickness of 750 to 850 Å. In this study, O additions to window layers fabricated at 250°C yield gains in V_{OC} and FF. In contrast, previous studies found a gain in J_{SC} when O additions were made to window layers deposited at room temperature. Figure 9 demonstrates that combinatorial approaches for optimization are possible, combining non-uniformity of the deposition over the area of the substrate with spectroscopic ellipsometry for mapping over the same area for characterization.

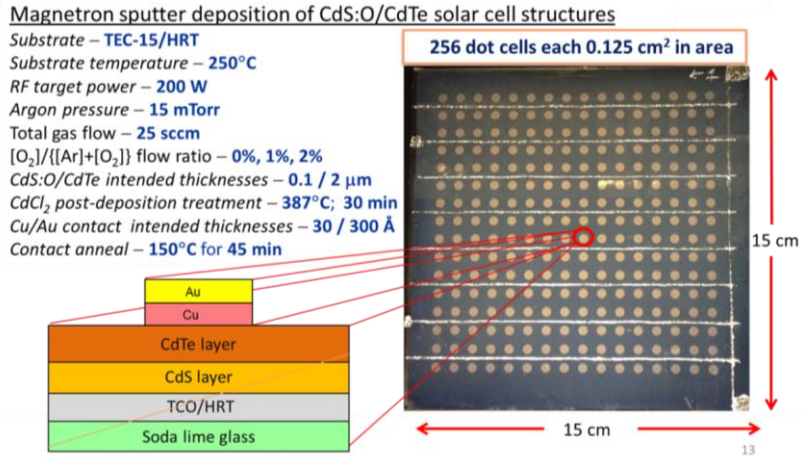

Figure 8. Fabrication conditions and standard layer structure for CdTe solar cells incorporating $CdS_{1-x}O_x$ for different flow ratios of $[O_2]/\{[O_2] + [Ar]\}$ during reactive sputtering.

New techniques are also being developed to probe the electrical properties of individual layers in a contactless manner using infrared and terahertz spectroscopic ellipsometry (SE) methods. For

example, when CdS is deposited on TEC-15/HRT substrates, standard co-planar conductivity measurements cannot be used to deduce the CdS properties due to the high conductance of the underlying SnO_2:F layer. Instead, the free carrier properties of CdS can be probed using infrared SE. For contactless analysis of free carriers in CdTe, the terahertz range is required due to the lower carrier concentration. Table 4 shows the properties of $CdS_{1-x}O_x$ films deposited in the solar cell configuration. The CdS deposition performed at a ratio of $[O_2]/\{[O_2] + [Ar]\} = 0.1$ exhibits the combination of the longest free carrier relaxation time τ and a high film density (as indicated by the high Cauchy amplitude).

(iii) *Advanced Metrology for the Photovoltaics Industry*

In supplying solar cell devices to the team, additional emphasis has been placed on advancing effective optical metrologies for the characterization of these devices. The metrologies developed in this project are being transferred to leading industry partners in multiple collaborations. Multichannel spectroscopic ellipsometry is a proven optical characterization technique for high speed multilayer analysis over a wide spectral range – from the near-infrared to ultraviolet (0.75 – 6.5 eV). CdTe solar cells in the superstrate configuration, however, exhibit considerable surface roughness which makes the film side ellipsometric measurement impossible. We have developed and continue to improve a technique that employs a glass side measurement, called "through-the glass spectroscopic ellipsometry". The advantage of this technique is that it can be applied to characterize partially completed plates as well as the final modules. In the latter application, it has sufficient analytical power to predict the external

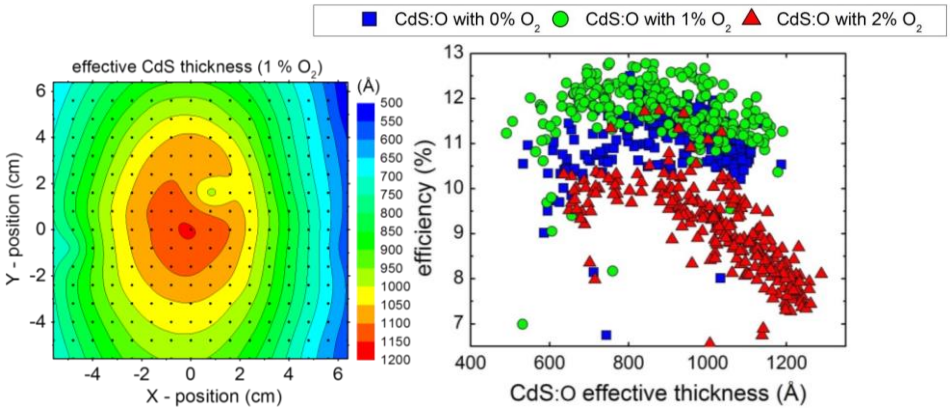

Figure 9. (Left) Map of $CdS_{1-x}O_x$ effective thickness (volume of film per area of substrate) as obtained by through-the-glass spectroscopic ellipsometry on the completed solar cell sturcture consisting of 256 dot cells; (right) cell efficiency plotted as a function of $CdS_{1-x}O_x$ thickness obtained by spatially correlating thickness and efficiency maps for three depositions with different flow ratios of $[O_2]/\{[O_2] + [Ar]\}$ during reactive sputtering of CdS.

Table 4. Characteristics of $CdS_{1-x}O_x$ films sputtered with different flow ratios of $[O_2]/\{[O_2] + [Ar]\}$ (first row) as obtained by infrared SE. In the table, ρ is the resistivity, τ is the free carrier relaxation time, and *A* is the Cauchy amplitude which scales with the film density.

$[O_2]/\{[Ar]+[O_2]\}$		0%	1%	2%	3%	4%
Drude characteristics	ρ (x 10^{-4} Ω-cm)	342.68 ± 11.8	149.63 ± 2.1	109.51 ± 0.7	93.1 ± 0.91	83.92 ± 0.61
	τ (fs)	2.84 ± 0.14	5.83 ± 0.09	4.023 ± 0.0364	4.77 ± 0.057	2.25 ± 0.037
Carrier concentration ($m^*= 0.25m_e$)	N (10^{19} cm^{-3})	0.915	1.02	2.02	2.01	4.72
Cauchy amplitude	A (unitless)	2.16 ± 0.009	2.31 ± 0.004	2.29 ± 0.004	2.24 ± 0.006	2.30 ± 0.01
Thickness (Å)		441.06 ± 1.44	475.19 ± 1.11	471.2 ± 0.923	485.35 ± 1.19	482.14 ± 2.2

quantum efficiency (QE) and all optical losses. Comparisons with the measured QE provides insights into electronic losses. Figure 10 (left) shows a best fit to SE spectra deduced in through-the-glass SE. The best fit structural parameters, including layer thicknesses and volume fractions associated with interface roughness and intermixing between layers, are shown in the top right schematic. The structural parameters extracted for this technique compare well with the values obtained by XTEM (Figure 10, lower right). Figure 11 shows the external QE simulated using the optical model of Figure 10 (solid line) in comparison with that measured at 0 V (dot-dashed line). In addition to the model parameter used from Figure 10 in the simulation, three assumptions were made: (i) complete collection from the 31 nm CdS/CdTe interface layer, (ii) 99% collection from the CdTe bulk layer, and (iii) 30% collection from the CdTe component of the 0.184 μm CdTe/Au interface layer, as shown in the schematic of the inset. Further support for the model (in addition to the good agreement between the simulation and the measurement) is obtained by performing QE measurements under reverse bias, which is found to be consistent with 100% collection from the bulk CdTe layer as well as from the CdTe component of the 0.184 μm CdTe/Au interface layer. The results of Figure 11 suggest carrier loss from the CdTe near the back contact, and an additional mdeling tool for evaluating the quality of the back contact.

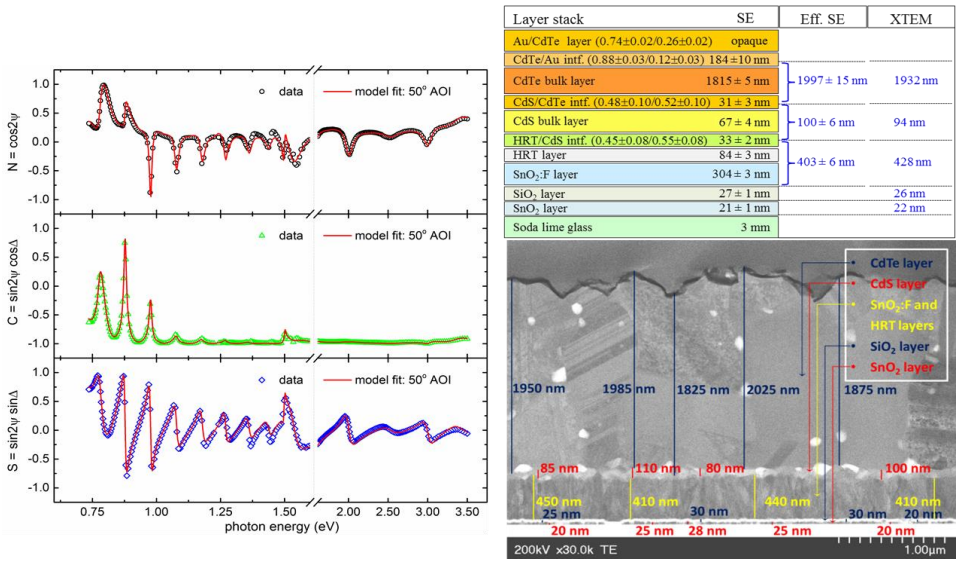

Figure 10. (Left) Spectroscopic ellipsometry data and best fit for a completed baseline ~ 12% CdTe solar cell measured on top of the back contact; (upper right) structural parameters deduced in the best fit to the SE data, including thicknesses and interface layer volume fractions, along with thickness comparisons to XTEM results; (lower right) XTEM image for the same sample.

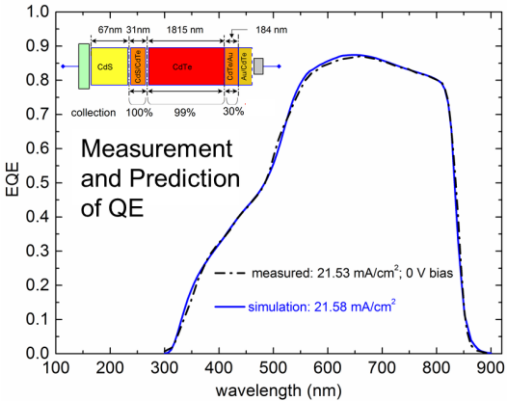

Figure 11. Quantum efficiency (QE) spectrum measured at 0 V (dot-dashed line) and that simulated based on the model of Figure 10. The model includes: (i) complete collection from the 31 nm CdS/CdTe interface layer, (ii) 99% collection from the CdTe bulk layer, and (iii) 30% collection from the 0.184 µm CdTe/Au interface layer, as shown in the schematic of the inset.

I.2.2 Subtask 2: Deposition of novel back contact materials.

Novel back contact materials will be deposited at UI and ODU on baseline CdTe solar cells without back contacts.

Transition metal nitrides such as ZrN are appealing as potentila back contacts to CdTe/CdS photovoltaics as they can be produced in large areas for low costs at high rates by reactive sputtering. Furthermore they have high chemical and thermal stability. Nitrides have been studied as back contacts to Cu(In, Ga)Se_2 (CIGS) solar cells. For example, Mahieu *et al*. deposited TiN by reactive sputtering and found improved current collection due to the high nitride reflectivity. This was confirmed by Malmstrom *et al*. who obtained increasing quantum efficiency at long wavelengths for 0.5 µm-thick CIGS with a ZrN back reflector compared to a conventional Mo back contact. Schleussner *et al*. deposited ZrN by dc magnetron sputtering for application in CIGS solar cells and demonstrated low resistivity contacts with better reflectance than Mo. Guo *et al*. studied TiN contacts to CIGS solar cells prepared by hollow cathode sputtering and obtained low resistivity (53 µΩ·cm) films and good cell cell efficiencies.

Commented [AR1]: From Zhenfeng's thesis

The most important parameter for a contact to CdTe is work function due to the high electron affinity of CdTe. Fujii *et al*. and Matenoglou *et al*., for example, determined the work functions of selected transition metal nitrides to be ~4.7, 4.8, 5.1, and 5.2 eV for ZrN, HfN, VN and TiN, respectively, although literature values for these quantities vary with deposition conditions and stoichiometry. These values are similar to current materials used as contacts to CdTe such as Mo (4.5 eV), Cu or Au (5.1 eV). Therefore all of these nitrides represent potentially interesting contact materials with high stability and ease of fabrication.

In general transition metal nitrides have low resistivities, in some cases lower than the parent transition metals, with values in the range of 10—30 µΩ·cm. Their high conductivity has been attributed to the high density of states at/near the Fermi level associated with overlap of the N p-orbitals with the transition metal d orbitals. For comparison, the lowest resistivity metals include Ag at 1.59 µΩ·cm and Al at 2.82 µΩ·cm.

Deliverables:

a. Demonstration of active solar cells using novel contacts of:
   i. Quarters 1-3: $CuInSe_2$
   ii. Quarters 3-6: Silicon

I.2.3 Subtask 3: Testing and modeling of solar cells.

The solar cells produced in the preceding tasks, with both baseline and novel contacts, will be tested by temperature-dependent light and dark current/voltage measurements to demonstrate changes to the back contact performance and the results will be quantitatively modeled to extract the Schottky barrier heights and built-in electric field in the device.

Deliverables:

a. Temperature-dependent light and dark current/voltage measurements of the solar cells produced above. Other tests will be performed as needed.
b. Modeling and analysis of the data and determination of Schottky barrier heights and diode properties including built-in voltage.
c. Preparation of an abstract describing the results of the work submitted to the 2013 IEEE Photovoltaic Specialists Conference.

(a) University of Illinois Activities in CdTe Solar Fabrication with Chalcopyrite Back Contacts

For the studies here, CdTe/CdS solar cells without back contacts were fabricated at the University of Toledo as described above. The samples were cleaved into 12.5 mm x 12.5 mm individual devices for contact deposition. The majority of studied under this project concerned ZrN. VN and HfN were also studied but was found to produce similar results.

ZrN films were produced by reactive magnetron sputtering in an ultrahigh vacuum (UHV) system with a load lock for sample insertion. The nitride contacts were deposited directly on the rear (CdTe) surface of the devices without heating. A mask with a circular or square opening was used to define the contact areas. Growth parameters were as described by Mei *et al*. at a rate of 40 nm/min, a sputtering power of 100 W in a 20 mTorr, 1.75% N_2 + 98.25% Ar gas mixture. Film thickness was measured using a Sloan Dektak surface profilometer and a four point probe measured the sheet resistivity of reference films deposited on Si (100). In some cases a 20 sec N_2 plasma pre-treatment was applied to the CdTe prior to the growth of the nitride film. A bias voltage of -30V to -80V was applied to the substrate to provide sputter cleaning and potentially N doping of the CdTe prior to contact formation. For selected studies a thin (2-20 nm) layer of Cu was deposited on the CdTe in a separate chamber. The samples were transferred to the nitride deposition system as quickly as possible to minimize oxidation of the Cu. In addition, in some experiments, contacts were annealed at 150°C to 400°C in dry N_2 for 30 minutes in a tube furnace.

Nitride films deposited on Si substrates and the CdTe solar cells were characterized by x-ray diffraction using a Phillips X'Pert diffractometer with Cu-Kα_1 radiation and thin film parallel plate collimator secondary optics. Hitachi S4800 or S4700 SEMs or an Asylum Research MFP-3D AFM were used to acquire surface morphologies. Samples analyzed by TEM were prepared by focused ion beam in a FEI Helios 600i. and analysed in a JEOL 2010 LaB6 electron microscope with a 200 keV electron beam. Scanning transmission electron microscopy (STEM) was conducted in a JEOL 2010F under conditions yielding an ~1 nm beam. Film compositions measured by EDS in the SEM or TEM instruments or by secondary ion mass spectrometry (SIMS) for relative changes in composition with depth. EDS data was quantified using the AZtecTEM software package. X-ray photoelectron spectroscopy (XPS) was used to determine the work function of the nitrides and the amount of Cu deposited on the CdTe films using a

Kratos Axis Ultra with a monochromatic Cu-$K\alpha_1$ excitation source. For optical properties of the contact layers, a Varian Cary 5G spectrophotometer and a J.A Woollam VASE ellipsometer were employed. Complete devices fabricated at the University of Toledo with Cu/Au back contacts were studied for comparison. Dark and light J-V characteristics were measured using an IV16 solar cell measurement system calibrated using calibrated crystalline Si cells. The illuminated area was 16 cm × 16 cm at 100 mW/cm^2. Some devices were also characterized at the University of Toledo using their equipment.

A 5 μm x 5 μm AFM image of a 200 nm thick ZrN film deposited on Si (100) showed a uniform surface with negligible roughness (near the noise limit). The film resistivity on Si was 12.3 to 22.0 μΩ-cm, consistent with previous reports and similar to good metals. However, films on CdTe showed much higher and variable in-plane resistivities of 10^3 to 10^6 Ω-cm. We conclude that the values on Si represent the true resistivity that would be consistent with through-nitride conduction. Series resistance due to the nitride was not observed in the current study. The films on CdTe were limited by the CdTe roughness but penetrated into or filled in pits and surface features to some extent. An example is shown in Figure 12.

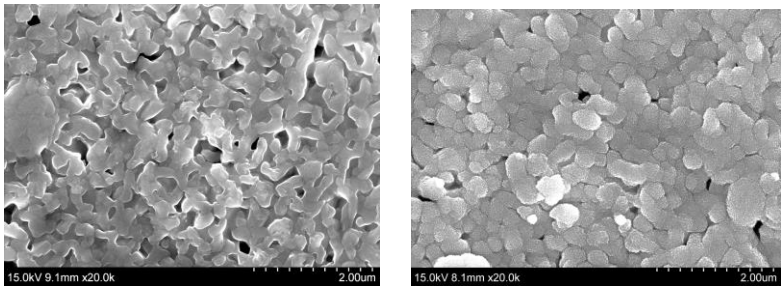

Figure 12: The CdTe surface observed by SEM before (left) and after (right) 200 nm of ZrN deposition.

Table 5 The parameters of effect of ZrN films thickness on the performance of CdTe/CdS solar cells.

Thickness (nm)	V_{oc} (V)	J_{sc} (mA/cm^2)	FF (%)	Efficiency (%)	R_s (μ-cm^2)	R_{sh} (μ-cm^2)	P_{Max} (mW)
90	0.228	3.909	25.198	0.225	57.735	61.401	0.028
140	0.155	9.849	26.316	0.402	14.058	16.478	0.05
250	0.269	16.389	32.088	1.414	11.318	31.45	0.177

Device performance was studied for different thicknesses of ZrN. The results are given in Table 5. Device performance improved with ZrN film thickness up to 250 nm. Thicker ZrN films tended to peel off the CdTe and reduce performance. All films showed low current and fill factor, although the thickest contact produced the highest current. The variation in V_{oc} for different ZrN thicknesses suggests that the devices were limited by problems with processing as no current flows in the contact at V_{oc}. Likewise, larger contacts covering the entire back surface of the device yielded lower performance devices than contacts covering only a portion of the device (4 mm diameter circular contact on a 12.5 mm x 12.5 mm sample). Low performance not associated with the contact itself was a persistent problem with contacts produced other than at the University of Toledo. Therefore later in the project period more emphasis was placed on making contacts by the Toledo group and study of the materials and device properties was emphasized at Urbana and Old Dominion.

Annealing the CdTe below 270°C °C shows no significant effect on surface morphology. At higher temperatures, significant changes in CdTe morphology occurs. For films covered with ZrN the changes were smaller, including at 270°C.

Addition of a thin layer of Cu to the back of the device prior to deposition of the nitride contact improved the device performance dramatically, as is the case with other contact metallizations. Both V_{oc} and J_{sc} improved, although the improvement in V_{oc} was most dramatic. Cu was deposited by sputtering at a rate of ~4 nm/min. The samples were transferred to the nitride deposition system and coated with ZrN at ~300°C, which permitted significant Cu diffusion during the nitride deposition. SIMS analysis showed that prior to ZrN deposition the Cu was highly localized at the surface of the CdTe, while after ZrN the Cu had migrated far into the film, as expected. Typical SIMS profiles are shown in Figure 13

The greatest improvement was found for the shortest deposition time tested (30 sec or ~2 nm of Cu) resulting in a V_{oc} of ~420 mV. This decreased with increasing amounts of Cu deposition to 270 mV for 12 nm of Cu and resulting in shorted devices for longer deposition times. Little or no improvement in fill factor was observed with Cu addition.

(a)

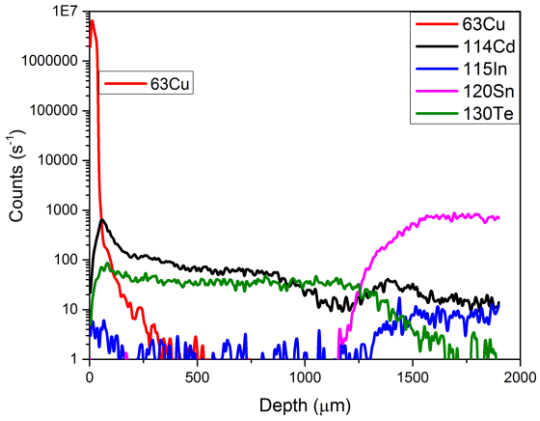

(b)

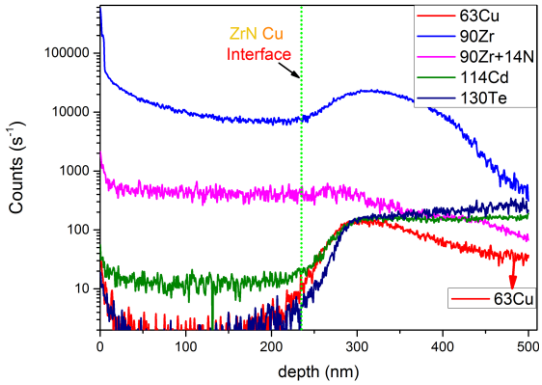

Figure 13: SIMS depth profiles showing the Cu distribution on CdTe devices (a) as deposited and (b) after deposition of ZrN at 300°C. The profile in (a) is nearly limited by the depth resolution of the instrument, although the tail of the profile at low count rates may represent real diffusion of Cu at room

The ZrN films are a golden color with metallic reflectivity. Indeed the reflection at short wavelengths below 800 nm (relevant to the CdTe devices) was higher than the standard Cu/Au back contact (Figure 14). We were not able to demonstrate a higher J_{sc} overall from the contacts produced for this project as a result of improved ZrN reflectivity because the devices produced were simply not as good as devices produced at the University of Toledo. However, the

transmission of the devices was significantly reduced relative to those with the normal Cu/Au contacts so we anticipate that with proper optimization the ZrN contacts could have produced a net improvement in the device, if nothing else as a reflector behind the normal contact.

(a)

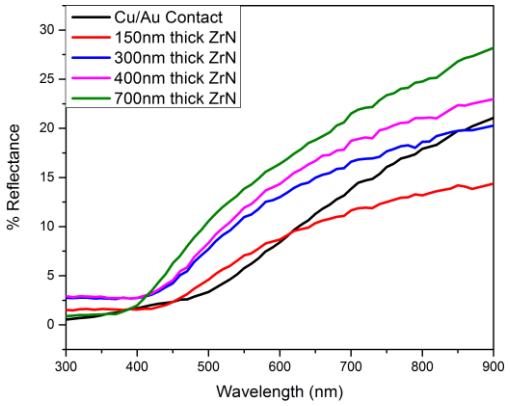

(b)

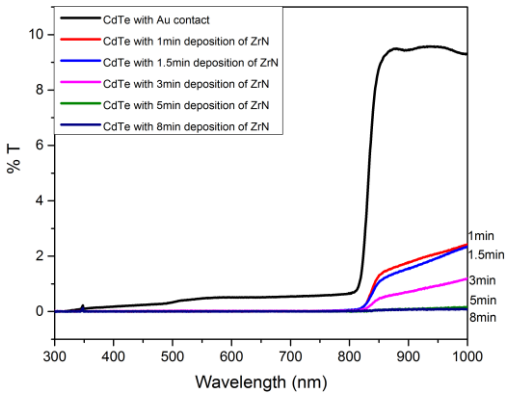

Figure 14: shows (a) the reflectance of the contact materials over the range of wavelengths relevant to the device and (b) the overall transmission of the device with the standard Cu/Au contact and with various thicknesses of ZrN. Even for very thin ZrN the reflectance is greatly improved

The ZrN contacts to CdTe were studied by transmission electron microscopy. The films were found to exhibit a halite crystal structure. Selected area diffraction patterns obtained from the

film suggested that the films had a (111) texture, although all of the expected grain orientations were observed. The ZrN/CdTe interface was abrupt, although an ~2 nm wide amorphous region was found in the ZrN at the CdTe interface. This thin amorphous layer probably did not significantly influence the contact resistance.

Finally, we examined the effect of treating the surface of the CdTe with a nitrogen plasma prior to deposition of the ZrN in an attempt to enhance doping through the interaction with N. The sample was biased at -30 or -80 V with respect to ground to attract the positive N ions in the sputtering discharge. After the plasma treatment, 200 nm of ZrN was deposited. No change in surface morphology of the CdTe was observed following plasma treatment and no second phases were evident. However, all of the resulting devices were shorted. The explanation for the shorted devices is not clear because there was no evidence of pinholes or other problems with the device layers. The lack of a change in observable microstructure was inconsistent with some sort of etching process.

(b) University of Toledo Activities in CdTe Solar Fabrication with Chalcopyrite Back Contacts

Table 6 summarizes the performance parameters for the devices completed with novel CIS contacts as compared to those completed with the UT standard Cu/Au back contacts. The devices used for the application of novel contacts were both sputter deposited and close space sublimated (CSS) CdTe devices. These devices with standard Cu/Au back contact have efficiencies in the range of 12.5% to 14.5%. Maximum efficiencies obtained in these processes are 13.5 and 16%, respectively. Working CdTe superstrate devices using CIS materials as novel back contacts were obtained. The performance of the devices with novel back contact materials is rather poor, however, as compared with devices having the standard Cu/Au back contacts. Devices made by the application of CIS by spray pyrolysis, even without N doping, showed improved performance over the devices made by applying CIS:N layer deposited by hybrid physical vapor deposition. The CIS back layer deposited by the wet process on the devices fabricated with sputter deposited CdTe showed slightly better performance as a back contact than that on the devices with CSS CdTe.

Table 6. Performance parameters for the devices fabricated by depositing $CuInSe_2$ layers by different processes have been compared. Standard device performance parameters have also been indicated in the table.

Device	J_{SC} **(mA/cm^2)**	V_{OC} **(V)**	***FF*** **(%)**	**Eff. (%)**	**Series res. (Ω-cm^2)**
CdTe by sputtering					
Std. Cu/Au	22.0	0.803	71.2	12.59	3.70
CIS:N	14.0	0.465	39.1	2.54	11.56
CIS (spray dep.)	19.8	0.675	47.6	6.36	20.17
CdTe by close space sublimation					
Std. Cu/Au	25.3	0.803	70.5	14.24	2.53
CIS:N	16.8	0.469	32.7	2.51	12.16
CIS (spray dep.)	22.8	0.671	40.2	6.13	21.34

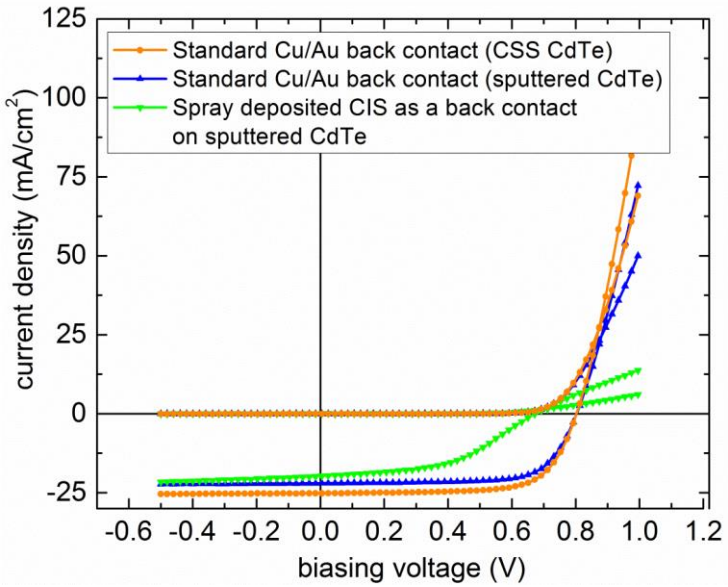

Figure 15. Light and dark J-V curves are compared for CdTe solar cells with the best CIS back contact with standard Cu/Au back contacts. The curves with circular symbols (orange) and upright triangles (blue) are for cells with CSS CdTe and sputtered CdTe absorbers respectively, both with Cu/Au back contacts. The curves with inverted triangles (green) are for the best cell with a CIS back contact, which was deposited by wet process.

Figures 15 and 16 present the *J-V* characteristics and quantum efficiency spectra for standard Cu/Au devices and one of the best performing cells with novel back contact. Problems were encountered in isolating the individual dot cells with CIS back contacts. As a result, large erroneous short-circuit currents were found for some of the devices. In such cases, the short circuit current values were determined from quantum efficiency measurement. Because of this reason, Figure 15 lacks *J-V* curves for the some of the cells of Table 6 with CIS back contacts.

The deposition of *p*-type semiconducting material, for example nitrogen doped CIS which is the focus of the proposed effort, involves heating the substrate to an elevated temperature (> 500°C). The application of such a layer as a back contact in the superstrate configuration results in the undesirable evaporation of the CdS/CdTe solar cell within the high vacuum environment, making the high temperature process impossible. The issue could be resolved by inverting the CdTe cell to the substrate configuration, enabling deposition of the CdTe absorber layer on a

substrate that has been previously coated with the doped CIS back contact layer. The inversion of the CdTe solar cell structure results in added challenges in the device fabrication. In order to evaluate back contact performance in this configuration, a baseline must be established. The research reported in the second phase is an attempt to develop an optimized baseline for CdTe device in the substrate configuration.

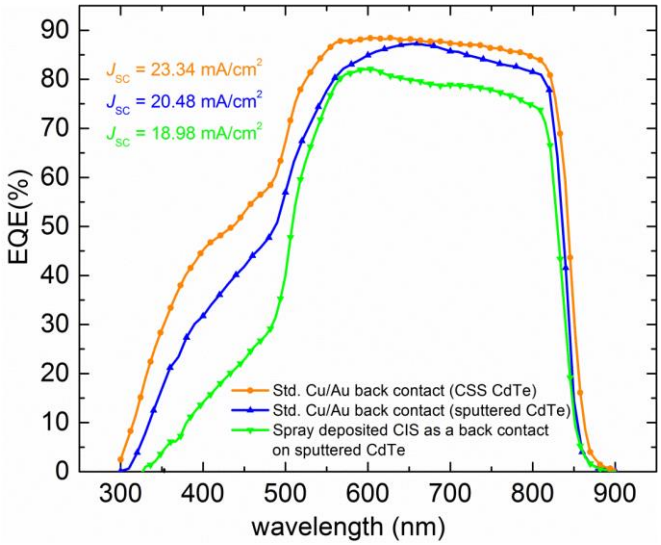

Figure 16. Quantum efficiency spectra are compared for CdTe solar cells with CIS back contacts and standard Cu/Au back contacts. The curves with circular symbols (orange) and upright (blue) triangles are for cells with CSS CdTe device and sputtered CdTe absorbers, respectively, both with Cu/Au back contact. The curve with inverted triangles (green) are for CIS back contact as deposited by the wet process on a cell with a sputtered CdTe absorber.

(a) University of Toledo Activities in CdTe Solar Fabrication with Silicon Back Contacts

The best CdTe solar cell performance was obtained using a-$Si_{1-x}C_x$:H:B back contacts whose deposition conditions were set for optimization of the hydrogenated amorphous silicon p-i-n solar cell efficiency when applied as the top *p*-type layer. The light and dark current density versus voltage (*J-V*) characteristics are shown in Figure 17 for two of the highest efficiency solar cells with a-$Si_{1-x}C_x$:H:B back contacts and for a cell with the standard Cu/Au back contact. For one of the cells, the a-$Si_{1-x}C_x$:H:B *p*-layer back contact was deposited on an as-$CdCl_2$-treated surface, and for the other cell, the $CdCl_2$-treated surface was exposed to a Br_2/methanol (MeOH)

etch prior to back contact deposition. Otherwise the fabrication conditions of the two solar cells were the same as described earlier.

Table 7 lists the performance parameters for the three cells of Fig 17. Among the CdTe cells with a-$Si_{1-x}C_x$:H:B back contacts, a best initial V_{oc} value of 0.75 V was obtained for a cell with the back contact on the Br_2/MeOH etched surface, yielding an efficiency of 7.3%. The best cell using the as-treated surface exhibited a lower V_{OC} value of 0.71 V but higher FF, yielding a

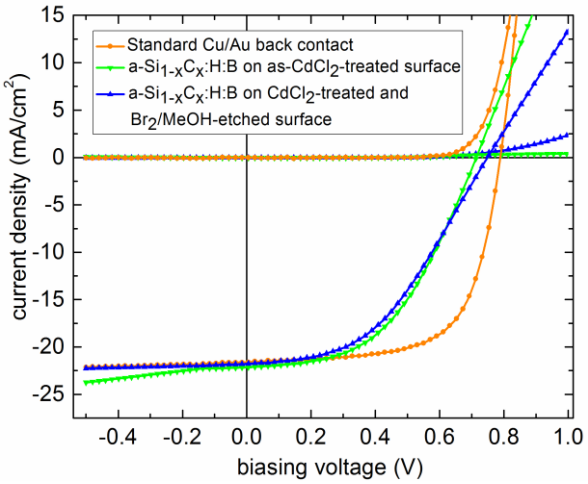

Figure 17. Light and dark *J-V* curves have been compared for CdTe solar cells with a-$Si_{1-x}C_x$:H:B/Cr back contacts and standard Cu/Au back contacts. The curves with inverted (green) and upright (blue) triangles are for cells with a-$Si_{1-x}C_x$:H:B/Cr back contacts on as-$CdCl_2$-treated and $CdCl_2$-treated + Br_2/methanol etched surfaces, respectively. The curve with the circular symbols (orange) describes a standard device. Devices with the novel back contacts show comparable V_{OC} and J_{SC} but reduced fill factor relative to standard devices.

maximum efficiency of 7.7%. A slight increase in series resistance is observed when the $CdCl_2$-treated CdTe is etched by Br_2/MeOH prior to deposition of the a-$Si_{1-x}C_x$:H:B back contact. The low efficiency of the cells with the novel back contacts relative to those with standard Cu/Au contacts is due to a low fill-factor generated by a high series resistance. The two cells with a-$Si_{1-x}C_x$:H:B back contacts in Figure 17 exhibit non-superposition of light and dark J-V characteristics, which can be attributed to a higher back barrier for these contacts. It should be emphasized that no Cu was introduced into the CdTe/a-$Si_{1-x}C_x$:H:B back contact for these cells.

Thus, under the optimized a-$Si_{1-x}C_x$:H:B *p*-layer conditions, similar CdTe solar cell performance is obtained for a-$Si_{1-x}C_x$:H p-layer back contacts deposited on $CdCl_2$-treated surfaces

exposed to the Br_2/MeOH etch and on as-$CdCl_2$-treated surfaces. The etch removes oxide arising from the $CdCl_2$ treatment, smoothens the surface, but leaves a thin a-Te layer. It is likely that the hydride gas plasma exposure during a-$Si_{1-x}C_x$:H:B deposition also serves to remove the top layers of the CdTe film, possibly accounting for the similar results. A study to evaluate the possible effects of hydride plasma on the surface of $CdCl_2$-treated CdTe is provided later in this report.

Table 7 Performance parameters are listed in the table for the devices with standard Cu/Au and a-$Si_{1-x}C_x$:H:B/Cr back contacts. Also included in the table are the *J-V* parameters of an H_2 plasma exposed CdTe device in comparison with a standard unexposed device from the same study.

Device	J_{SC} **(mA/cm^2)**	V_{OC} **(V)**	***FF*** **(%)**	**Eff. (%)**	R_s **(Ω cm^2)**
a-$Si_{1-x}C_x$:H:B/Cr back contact study					
Std. Cu/Au	21.6	0.788	67.0	11.41	5.3
a-$Si_{1-x}C_x$:H (as-$CdCl_2$-treated)	22.1	0.713	48.8	7.72	12.2
a-$Si_{1-x}C_x$:H (etched CdTe)	21.8	0.748	44.8	7.31	18.1
H_2 plasma exposure study					
No H_2 plasma exposure	22.9	0.781	67	12.07	4.6
H_2 plasma exposure	22.5	0.712	64	10.22	4.5

Quantum efficiency (QE) responses are shown in Figure 18 for three solar cells including two with a-$Si_{1-x}C_x$:H:B back contacts, with and without the etching step performed post-$CdCl_2$ treatment, and the third one with a standard Cu/Au back contact. The results for the cells with the a-$Si_{1-x}C_x$:H:B back contacts were obtained one week after cell fabrication. The effect of degradation of the solar cells over time will be discussed in greater detail in paragraphs to follow. The QE responses of all three cells in Figure 18 are similar over the range above 500 nm. The effect on the QE behavior of the etching step before a-$Si_{1-x}C_x$:H:B back contact formation is not significant, and the difference between the two spectra below 500 nm is due to a CdS thickness difference.

The downward slope in the QE in Figure 18 with increasing wavelength over the 700-800 nm range is attributed to electronic losses when photons are absorbed near the back contact. This slope is stronger for the two cells with a-$Si_{1-x}C_x$:H:B back contacts, suggesting greater losses near the back contact.

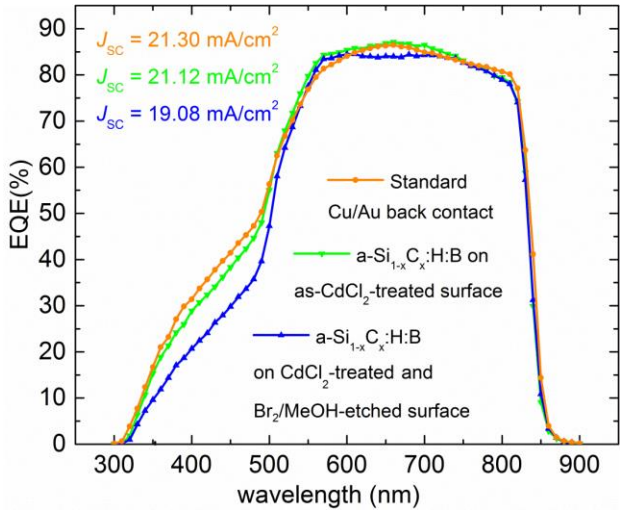

Figure 18. Quantum efficiency spectra are shown in the figure for two devices with a-$Si_{1-x}C_x$:H:B/Cr back contacts, with and without an etching step between the $CdCl_2$ treatment and back contact deposition (upright triangles, blue line; and inverted triangles green line, respectively). These measurements were performed one week after back contact deposition. These results are compared with a standard device having a Cu/Au back contact (circular points, orange line). The short circuit current values shown in the figure were calculated based on QE integrations.

I.2.4 Subtask 4: Heat treatment and stability of novel contacts

The solar cells produced in the preceding tasks, with both baseline and novel contacts, will be tested for stability of the contacts and devices based on accelerated lifetime tests and annealing to failure. Accelerated lifetime tests will follow standard protocols at UT for CdTe solar cells. Annealing studies will examine interdiffusion, reaction and other degradation mechanisms based on higher temperature anneals to understand the limits of contact performance.

The initial results shown in Figures 17 and 18 and Table 7 appeared promising and suggested that further optimization of the PECVD process was possible. In addition to these further optimization attempts, the long term stability of the first series of cells with the a-$Si_{1-x}C_x$:H:B back contacts was tracked. As a result, the performances of the two devices of Figure 17 and Table 7 have been measured at various intervals over a period of almost two years. Highest performing CdTe solar cells with a-$Si_{1-x}C_x$:H:B *p*-layer back contacts have been found to degrade significantly over time as shown in Figure 19. The degradation behavior for the performance parameters of the standard cell is shown in Figure 19 for comparison.

The primary effect observed for the cells with a-$Si_{1-x}C_x$:H p-layer back contacts is an increase in series resistance which degrades the fill-factor significantly. J_{SC} also degrades as was indicated by the QE study of Figure 18; however, V_{OC} is relatively stable and actually increases for the two best cells after one week's time. It is proposed that the degradation effect is due to diffusion primarily of H, but possibly of B as well, from the a-$Si_{1-x}C_x$:H:B into the CdTe. Loss of either H or B from the a-$Si_{1-x}C_x$:H:B closest to the CdTe would lead to a Fermi level shift in the contact layer toward midgap and to an increase in resistivity of this layer; however, it is interesting that there is no corresponding large effect on V_{OC} in the first week, that is, during the period of the most rapid drop in fill-factor.

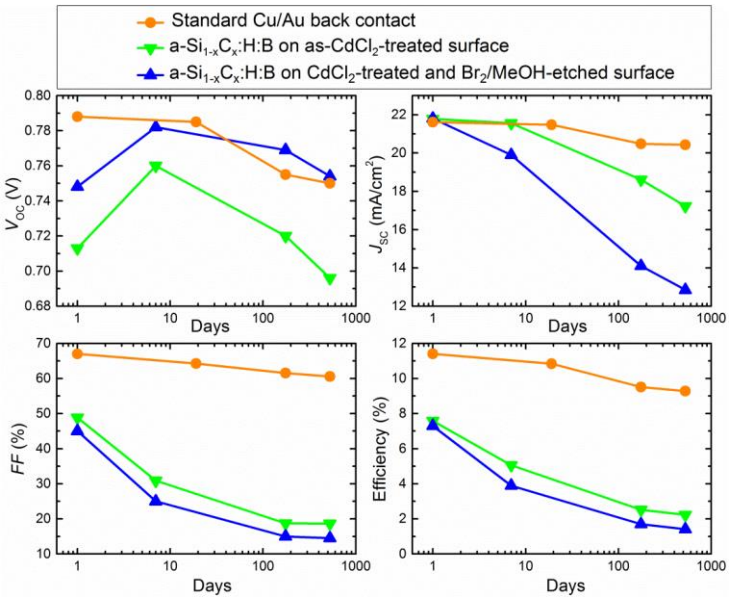

Figure 19. Degradation plots are shown for three CdTe devices observed over a time period of two years. The inverted triangular points (green lines) and upright triangular points (blue lines) indicate the performance parameters for devices with a-$Si_{1-x}C_x$:H:B/Cr back contacts on as-$CdCl_2$-treated and $CdCl_2$-treated + Br_2/methanol-etched surfaces, respectively. The circular symbols (orange lines) represent the parameters for a standard device with Cu/Au back contact.

Previous studies of the deposition of a-Si:H-based *p-i-n* superstrate solar cell structures have shown that H is unstable in a-$Si_{1-x}C_x$:H:B and evolves from the material immediately after its deposition at 200 °C. The H can be restored with a H_2 plasma just prior to *i*-layer deposition. Once the *p*-layer is capped by the a-Si:H *i*-layer, then the structure is stable presumably due to the ability of the underlying transparent conducting oxide to suppress H-diffusion and the

similarity of the atomic H chemical potentials of the *p*- and *i*-layers. In contrast, for the a-$Si_{1-x}C_x$:H *p*-layers on CdTe, the underlying semiconductor serves as a sink for H-diffusion that may continue over a long period of time as indicated in Figure 19.

In addition to a possible detrimental effect of H loss on the back contact layer properties, the diffusion of H from a-$Si_{1-x}C_x$:H:B into the CdTe is likely to modify the electronic properties of CdTe layer and, thus, the performance of the solar cell. To explore the possible effects of atomic H incorporation in CdTe, a $CdCl_2$-treated solar cell structure was exposed to a H_2 plasma for a very short time duration, 15 seconds, which is a factor of ten times shorter than the a-$Si_{1-x}C_x$:H:B p-layer deposition time. The goal of the H_2 plasma exposure is to simulate not only the possible effects of diffusion of H into the CdTe from the a-$Si_{1-x}C_x$:H:B back contact layer, but also the effects of hydride plasma exposure of the CdTe in the initial stages of growth of the a-$Si_{1-x}C_x$:H:B back contact layer. The H_2 plasma exposed cell structure and an unexposed control cell structure from the same process were completed with Cu/Au back contacts.

In a separate experiment designed to provide insights into the structural effects of the H_2 plasma, the CdTe surface was monitored by real time spectroscopic ellipsometry (RTSE) during H_2 plasma exposure. The exposure time was increased to 45 seconds (3 x longer than that used in the devices as described above) for a larger data set and a clearer understanding of the effect of the plasma in modifying the surface of the $CdCl_2$-treated device. RTSE analysis results shown in Figure 20 indicate that the CdTe bulk layer is etched at 1.3 Å/s during H_2 plasma exposure with a loss of ~ 60 Å during 45 sec. In addition, the void volume fraction in the 225 Å thick CdTe surface roughness layer increases from its initial value of 30 vol.% to 40 vol.% by the end of the exposure time . Thus, the total loss of CdTe effective thickness (or volume/area) is ~ 80 Å during the exposure time. Further study is needed to evaluate possible changes in the optical properties of the CdTe bulk layer or possible formation of a-Te within the surface roughness layer.

The performance parameter statistics for the solar cells with 15 s H_2 plasma exposure have been compared in Figure 21 with those of unexposed control cells. The parameters for a H_2 plasma exposed device and an unexposed device have been listed in Table 7. Figure 21 shows that the structure exposed to the H_2 plasma after $CdCl_2$ treatment incurs a reduction in the median and maximum performance parameters of V_{OC}, fill-factor, and efficiency relative to the standard control devices.

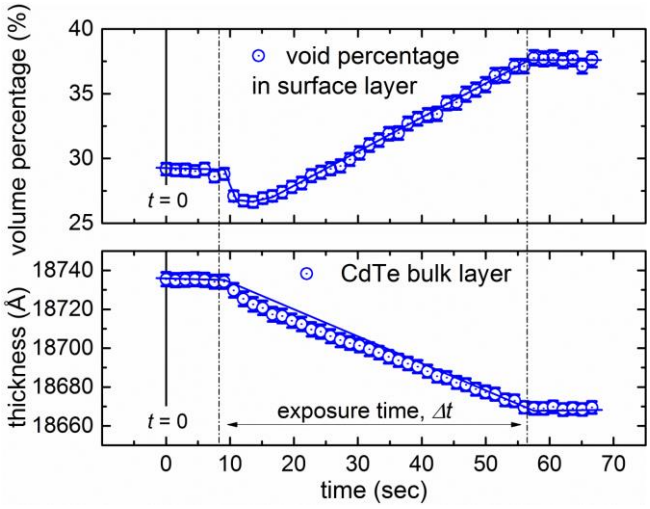

Figure 20. Results shown in the diagram correspond to the analysis of RTSE data collected during a $\Delta t \sim 45$ s H_2 plasma exposure of a $CdCl_2$-treated CdTe solar cell structure. The figure shows the void volume fraction in the 225 Å surface roughness layer (top) and the CdTe bulk layer thickness (bottom) during the time over which the device was exposed to the H_2 plasma.

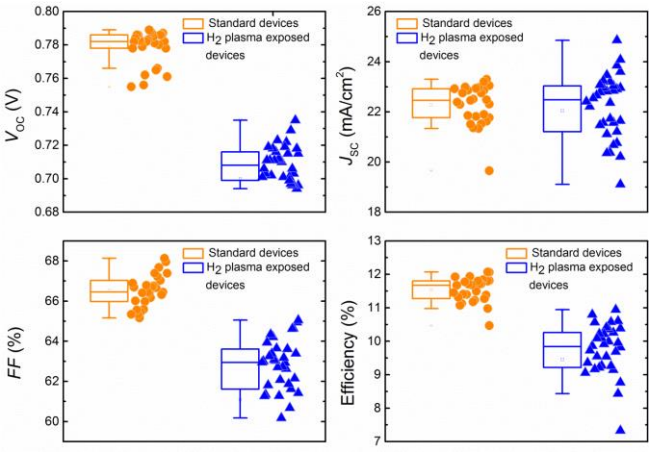

Figure 21. A comparison is made on statistical data for the performance parameters of the H_2 plasma exposed and standard CdTe devices. The boxes and circular symbols (orange) on the left side of each panel represent the standard CdTe devices and the boxes and triangular symbols (blue) on the right side represent the H_2 plasma exposed devices.

The drop in average V_{OC} due to H_2 plasma exposure is similar in magnitude to that observed for the as-$CdCl_2$-treated cell with the a-$Si_{1-x}C_x$:H:B back contact in long term stability studies; however, the drop in *FF* is relatively weak in comparison. This behavior suggests that it is degradation of the a-$Si_{1-x}C_x$:H:B layer itself that leads to the large increase in series resistance and to the primary instability, whereas the changes in V_{OC} can result from either loss of H from the back contact or incorporation of H via diffusion into the CdTe.

The detrimental effect of even a brief H_2 plasma exposure of $CdCl_2$-treated CdTe implies that it is impossible to fabricate thin film Si-based back contacts using plasmas of H_2-rich SiH_4 + H_2 mixtures. Such mixtures are necessary for the deposition of the highest quality amorphous and nanocrystalline (nc) Si:H p-layers at low temperatures. In fact, such attempts in the laboratory to generate nc-Si:H:B back contacts on CdTe have led to very poor performing cells, presumably due to the H_2 rich plasma exposure of CdTe. In fact, the problem of p-type Si:H-based film deposition on CdTe surfaces is similar to that of its deposition on transparent conducting oxide (TCO) coated glass in the *p-i-n* superstrate configuration -- due to the detrimental effects of atomic H on the underlying materials in both cases (CdTe and TCO surfaces).

Figure 22 shows the stability of the performance parameters of a solar cell obtained with H_2 plasma exposed CdTe over a period of ~ 2 months. Both V_{OC} and fill-factor show degradation over this period relative to the unexposed samples of Figure 19. This behavior suggests that atomic H incorporated in the CdTe from the H_2 plasma exposure is continuing to diffuse within the CdTe layer and modifying the material properties and device performance over long time periods.

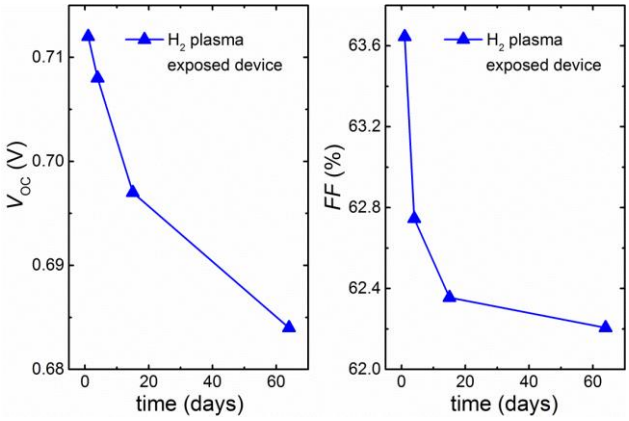

Figure 22. Degradation plots of V_{OC} (left) and FF (right) for the H_2-plasma exposed CdTe solar cells are shown in the diagram. The plasma exposure was 15 seconds in duration and was performed after the $CdCl_2$ treatment and before the Cu/Au back contact formation. The devices were measured at different times over a two month period.

The results in Figures 21 and 22 for H_2 plasma exposed devices in comparison with unexposed standard devices are attributed to the electronic behavior of H in interstitial sites in *p*-type CdTe. Interstitial H is expected to serve as a donor and compensate the native acceptors. This mechanism would lead to the decrease in *p*-type conductivity of the absorber layer and ultimately the observed decrease in overall device performance. The atomic H is likely playing a similar detrimental role in the performance and instability of CdTe solar cells with *p*-type a-$Si_{1-x}C_x$:H:B back contacts, whereby the H source is the hydride plasma exposure in the formation of the back contact, and diffusion from the back contact.

Downselection criteria

- Best CdTe solar cell
  - Stability
    - 90% of previous performance, 100 hrs at Voc, 0.7 suns, 65°C.
  - Highest quality contact (lowest Schottky barrier height, highest built-in voltage in the resulting cells)
  - Lowest process temperature

Downselection to reduce candidate materials to one or two materials to be examined in Phase II with the possibility to accept one or two materials with potential to be effective transparent conductors and one or two nitrides to be effective for substrate-geometry devices if there is strong motivation to choose different classes of materials for different benefits. No more than two candidate materials would be continued to Phase II.

Deliverable:

Quarter 6: Downselected materials for study in Phase II along with a justification for the choice(s).

Go/No-Go decision at the end of Phase I:

Failure of both of the following would suggest a no-go decision: (1) inability to demonstrate nitrogen doping of chalcogenide semiconductors, (2) no solar cell showing promising/improved contact behaviors with the novel materials.

(a) University of Toledo Activities in CdTe Solar Fabrication with Pyrite Back Contacts

Preliminary work on pyrite back contacts at UT motivated continuing study of this material in Phase II (see next section). The work on thin film Si:H back contacts was discontinued in Phase II due to the instability of the resulting back contacts. In the process of exploring new back contact materials for CdTe devices, the UT team collaborated with UT Prof. Ellingson's group to

apply Cu-free nanocrystalline (NC) pyrite (FeS_2) and in solar cell devices as a novel back contact material to supplement the continuing work on chalcopyrites ($CuInSe_2$). Unlike vacuum deposited CIS:N which requires heating the substrate at a temperature > 500°C, the FeS_2 NC film can be deposited by a drop-casting technique at room temperature and atmospheric pressure. FeS_2 NC synthesis involves solution-based thermal injection reaction, in the presence of trioctylphosphine oxide (TOPO) or 1, 2 hexanediol of an iron salt solution with an elemental sulfur source. Similar to CIS:N, the high hole concentration and low resistivity make FeS_2 a promising conductive and low barrier contact to CdTe. Figure 23 shows the schematic of non-interacting band diagram for the different layers in the CdTe solar cell device with respect to the vacuum level.

X-ray diffraction (XRD) and EDX measurements performed on the FeS_2 NC films indicated high purity FeS_2 with pure FeS_2 cubic phase. Electrical characterization of the films revealed that the films so prepared were p-type with carrier concentrations in the range of 10^{18} to 10^{19} cm^{-3}. Figure 24 shows an SEM image of a typical FeS_2 NC film.

For the application of this novel material in a device structure, samples were prepared by depositing the CdTe absorber layers by magnetron sputtering and by close space sublimation on high resistivity transparent (HRT) layer coated TEC-15 glass in turn coated with sputter deposited CdS. Devices were made by depositing ~ 1 μm thick NC FeS_2 layer by the drop-cast technique then evaporating a 300 Å thick gold layer as a final metal contact. Figure 25 shows schematics comparing device configurations for the standard Cu/Au and novel FeS_2 back contacts. Table 8 lists the average values for performance parameters of devices with sputtered CdS/CdTe window/absorber layers and three different back contact layers. The average is determined from fifteen dot cells each having an area of 0.085 cm^2. The results appear very promising in that the devices with novel back contacts *and no added Cu* exhibit comparable device performance parameters to those with standard Cu/Au back contacts. Figure 26 shows J-V characteristics and external quantum efficiency spectra for a typical dot cell of each of the three kinds.

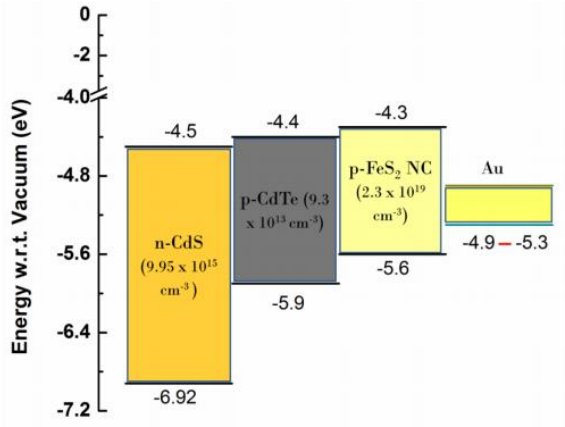

Figure 23. Non-interacting band diagram for the component layers of a CdTe solar cell structure with an FeS_2 back contact. The energy scale is plotted relative to the vacuum level indicated by 0 eV at the top.

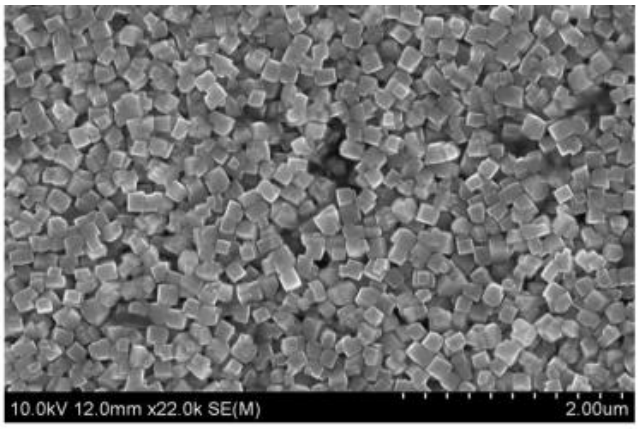

Figure 24. SEM image of an FeS_2 film deposited by drop-casting technique at room temperature and atmospheric pressure.

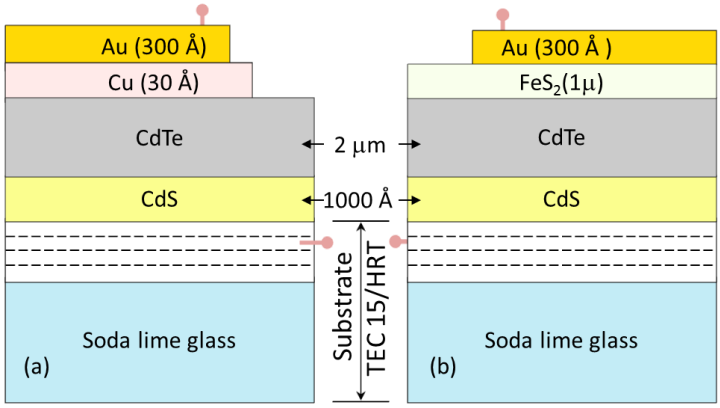

Figure 25. (a) Layer stack for the CdTe solar cell with a standard Cu/Au back contact; (b) layer stack for a CdTe cell with a novel p-type FeS_2 back contact and Au as the final metal contact to define the cell area. The thicknesses for CdS and CdTe layers indicated in the figure are typical for sputtered deposited devices.

Table 8. Average performance parameters for three device structures with Au, Cu/Au, and FeS_2/Au as the back contact materials. The devices used for these results incorporated sputter deposited CdS/CdTe layers. The average performance parameters were determined from fifteen dot cells each having an area of 0.085 cm^2. The FeS_2/Au back contacts were prepared without introducing Cu.

Back Contact	**V_{OC} (V)**	**Jsc (mA/cm^2)**	**Fill Factor (%)**	**Efficiency (%)**	**Series Res. ($\Omega\ cm^2$)**
Au	0.64±0.04	20.2±0.94	59.3±2.4	7.7±0.8	7.7±0.6
Cu/Au	0.79±0.02	21.8±0.67	65.4±1.9	11.3±0.9	5.4±0.9
FeS_2/Au	0.77±0.01	22.4±1.02	61.5±1.0	10.6±0.4	6.9±0.4

For the optimized performance of the devices, FeS_2 layers with varying thicknesses were applied in CSS CdTe devices. This work was an extension of the studies on sputtered cells and was done as a collaboration with Prof. Yan's group at UT. These devices with standard Cu/Au back contact demonstrated > 14 % efficiency under AM 1.5 illumination. In these studies, FeS_2 NC film thicknesses were varied over the range of 0.35 – 1.5 µm, fixing other structural parameters. All devices were completed with ~ 30 nm Au layer as the final metal contact and measured under one sun illumination. Figure 27 shows the J-V characteristics for the devices with different FeS_2 layer thicknesses and for a standard Cu/Au device. The results show that the device with ~ 0.7

μm thick FeS_2 layer performed the best among the other devices with different FeS_2 thicknesses in the series. Table 9 lists the performance parameters for the best performing devices of different types.

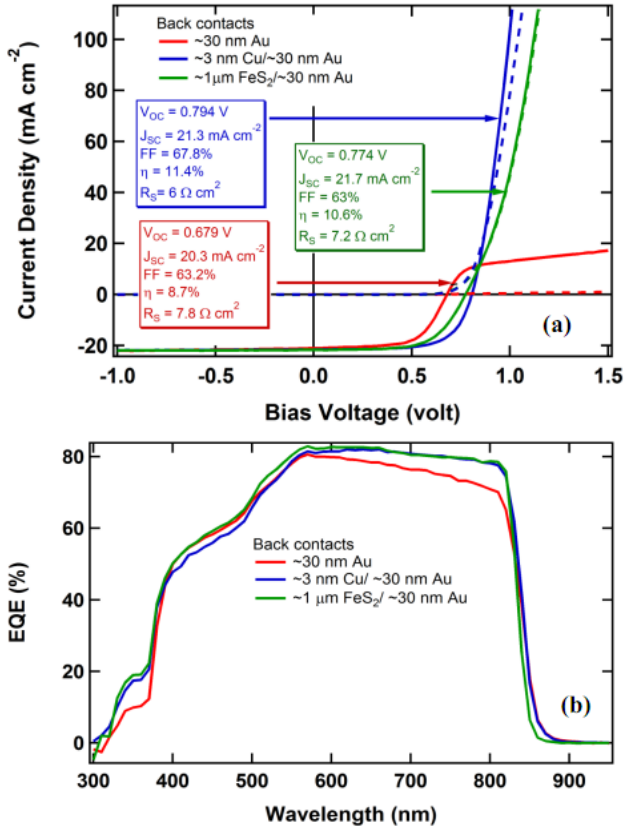

Figure 26. J-V characteristics in the light (solid lines) and dark (dotted lines) and (b) external quantum efficiencies for three typical dot cells having Au, Cu/Au, and FeS_2/Au back contact materials are indicated by red, blue and green curves. The absorber layers of these solar cells were fabricated by sputtering.

In summary, this work demonstrates the applicability of thin film nanocrystalline FeS_2 as a novel Cu-free back contact materials for CdTe solar cells. FeS_2 used in this work was intrinsically p-type. Future work in Phase 2 will focus on introducing Cu to these back contacts as well as

vacuum deposition of FeS_2 contacts using the hybrid method of Fe sputtering and S evaporation. This approach would be analogous to CIS hybid deposition, but easier to implement since the stoichiometry is not as demanding. Thus, ease of fabrication may be an advantage of the pyrite relative to the chalcopyrite. New results are presented in the next section.

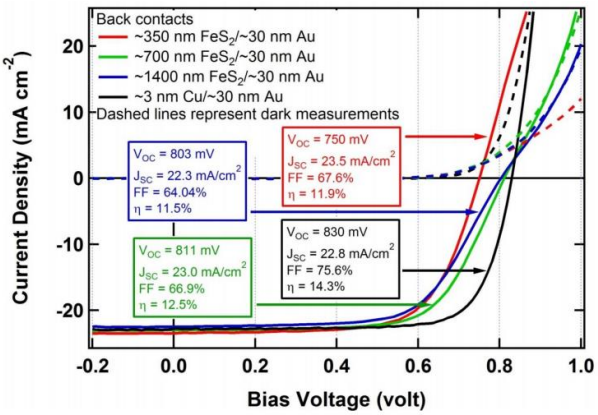

Figure 27. J-V characteristics -- light (solid lines) and dark (dotted lines) -- for devices with FeS_2 layer thicknesses ranging from 0.3 μm to 1.5 μm. Also shown in the diagram are the corresponding characteristics for a device with a standard Cu/Au back contact. These solar cells were fabricated with a CSS absorber layer.

Table 9. Performance parameters for the CdTe devices fabricated by sputter deposition and close space sublimation having different back contact layers. These parameters correspond to the best performing devices from the deposition series for each type.

	Voc (V)	**Jsc (mA/cm^2)**	**Fill Factor (%)**	**Efficiency (%)**
Sputtered CdTe, Au back contact	0.648	18.6	64.3	7.7
Sputtered CdTe, Cu/Au back contact	0.801	24.0	69.4	13.3
Sputtered CdTe, FeS_2/Au back contact	0.757	22.7	62.3	10.7
Sputtered CdTe, Cu/FeS_2/Au back contact	0.803	22.5	70.9	12.8
CSS CdTe, Cu/Au back contact	0.830	22.8	75.6	14.3
CSS CdTe, FeS_2/Au back contact	0.811	23.0	68.9	12.5

Phase II – Second 18 months

Phase II can be summarized as selecting one or two of the most promising materials demonstrated in Phase I and optimizing their performance to show the capabilities of the new materials. Phase II will also explore substrate-geometry devices based on sufficiently stable contact materials downselected in Phase I. While no contact material is likely to achieve its ultimate performance in a fully-optimized device within three years of beginning research, this phase will end with a clear evaluation of the prospects generally of the new materials and the downselected materials in particular, along with a roadmap to full optimization. We anticipate that by the end of the second phase we will be working directly with other research groups and manufacturers to extend the project and implement the technology in products. We anticipate that test products may be developed by manufacturers before the end of Phase II if the contacts prove sufficiently interesting.

Task #1 – *Demonstration of heavily p-type contact materials*

I.1.1 Subtask 1: Deposition and characterization of novel back contact material(s)

During Phase II we will conduct measurements on the downselected material(s) to determine the valence band and Fermi level for doped and undoped materials to show the change in electronic structure due to nitrogen addition. Measurements will include Kelvin-probe force microscopy, photoemission, photoluminescence, Auger electron spectroscopy, and other measurements as needed. Results will be checked for consistency with device results to show the nature of the contacts obtained.

Deliverables:

a. Determine the change in valence band behavior as a function of doping.
b. Determine the contact potential with respect to CdTe

I.1.2 Subtask 2: Demonstration of N-doping of chalcopyrite and delafossite materials.

We will continue to study and optimize doping of the downselected semiconductor(s) during Phase II and determine whether additional processing further enhances or reduces doping effectiveness.

Deliverables

a. Results of doping after contact annealing to optimize the contact material and determine the stability of conduction in the material.

b. Determine the effects of crystallinity on doping effectiveness and carrier mobility in polycrystalline contact materials.
c. A final analysis of the mechanism of doping, the defect levels produced, and the limits of solubility for the dopant in the various materials.
d. Determination of quantitative properties of the transparent conductor such as the plasma frequency as a function of doping density.
e. Publication of at least one paper describing the optimized properties of the material.

Task #2 – *Testing of novel contact materials in CdTe solar cells*

I.2.1 Subtask 1: Deposition of CdTe solar cells

During Phase II we will continue deposition of superstrate-geometry materials for testing of back contacts. Fabrication of substrate devices focusing on the material downselected at the end of Phase I for contact stability will be conducted during Phase II.

Deliverables:

a. Baseline superstrate type 14%-efficient CdTe solar cells with characterization of their general properties for continuing comparison with novel contact devices.
b. Superstrate type CdTe solar cells lacking back contacts delivered to UI and ODU groups.
c. Substrate-geometry devices fabricated on downselected contact materials optimized for stability with respect to CdTe. Back contacts for this portion of the project to be supplied by UI and ODU and fabricated on soda lime and/or borosilicate glass. Other substrates such as Si wafers may be used in some cases where tests require different processing conditions or different temperatures for which glasses are not suitable.

(a) University of Toledo Activities in Establishing a Baseline for CdTe Solar Cells in the Substrate Configuration

Figure 28 shows the layer stack developed for CdTe thin film solar cells in the substrate configuration. The fabrication steps involve sputter deposition of 0.80 μm of Mo at 250 ºC on borosilicate glass followed by the growth of a 800 Å MoO_3 layer by the atomic layer deposition (ALD) method. The sample thus prepared is overdeposited by 2 μm of CdTe using the magnetron sputtering process at 250 ºC. The structure is $CdCl_2$ treated, which involves applying $CdCl_2$/MeOH to the surface and annealing in dry air at 387 ºC for 30 min. The treated device is cleaned with methanol, and then overdeposited by CdS using chemical bath deposition (CBD) with the targeted

thickness of 1000 Å. The device is completed by depositing a bi-layer TCO which is ZnO/ZnO:Al followed by final metal contact. Table 10 summarizes the deposition parameters for the CdTe device in the substrate configuration. It should be emphasized that this is a Cu-free device.

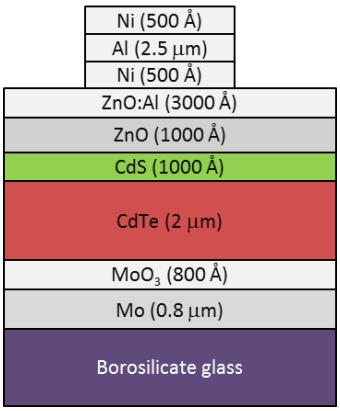

Figure 28. Layer stack for the CdTe thin film solar cell in the substrate configuration. All the layers other than MoO_3 and Ni/Al/Ni were deposited by sputtering. An 800 Å layer of MoO_3 was deposited by atomic layer deposition (ALD) on Mo coated borosilicate glass and final metal contact layers (Ni/Al/Ni) were deposited by e-beam evaporation.

Figure 29 shows the J-V characteristics under AM 1.5 for the best performing dot cell among 36 similar devices fabricated on a 5.1 cm x 5.1 cm substrate. For the same device, Figure 30 shows the external quantum efficiency (EQE) from which the short-circuit current (J_{sc}) was deduced as a more accurate value. The manual scribe-isolation of the individual dot cells results in possible inaccuracy in the area of the cells and consequently, inaccuracy in the J_{sc} calculated based on these areas. Our scribing process for the CdTe substrate process needs improvement in order to obtain better agreement between the two J_{sc} measurements. Hence, J_{sc} for the best performing cell was obtained from QE. The legend in Figure 29 shows the efficiency (6.86%) for the best performing device calculated from J_{sc} as obtained from QE measurement. Table 11 lists the device performance parameters for the best performing device (highest efficiency) and the highest V_{oc} device (for which QE measurements were not available).

CdTe thin film solar cells have been fabricated in substrate configuration, which resulted efficiency as high as 6.9 % and a V_{oc} as high as 0.66 V. The device parameters require ongoing optimized so that novel contact materials deposited at high temperatures can be evaluated. In addition, improvements are needed in scribing for this process to enable definitive measurements of short-circuit current and efficiency.

Table 10. Device fabrication parameters are tabulated for the CdTe solar cell in the substrate configuration. The process involves sputter deposition CdTe layers on borosilicate glass/Mo/MoO_3 substrates followed by a $CdCl_2$ treatment step for 30 min. The treated structure is coated with a 1000 Å CdS layer by chemical bath deposition (CBD). The device is completed by depositing a bi-layer of transparent conducting oxide (TCO) followed by electron beam evaporated grids.

Deposition Process and Parameters	**CdTe Layer**	**CdS Layer**
Substrate structure	BSG/Mo(0.8μm)/MoO_3(800Å)	1000 Å of CdS by chemical bath deposition
Deposition temperature	250°C	
Base pressure	1.6 x10^{-7} Torr	
Gas flow rate (Ar)	23 sccm	
Deposition Ar pressure	10 mTorr	
RF power	200 W	
Deposition time	120 minutes	
Intended thickness	2 μm	
$CdCl_2$ treatment	saturated aqueous solution applied to CdTe surface; heated in 0.5 ft^3/min of dry air for 30 min at 387°C	
ZnO/ZnO:Al	1000/3000 Å (sputtering)	
Ni/Al/Ni	500 Å /2.5 μm/ 500 Å (e-beam evaporation	

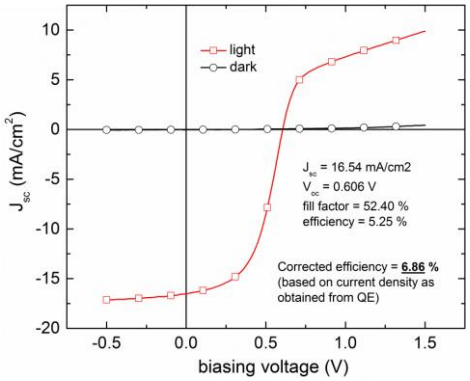

Figure 29. Light and dark J-V characteristics for the best performing cell among 36 dot cells fabricated on a 5.1 cm x 5.1 cm glass/Mo/MoO_3 substrate under AM 1.5 illumination. Indicated in the figure are the efficiencies calculated based on current densities as measured from J-V characteristics (5.25 %) as well as from QE (6.86 %).

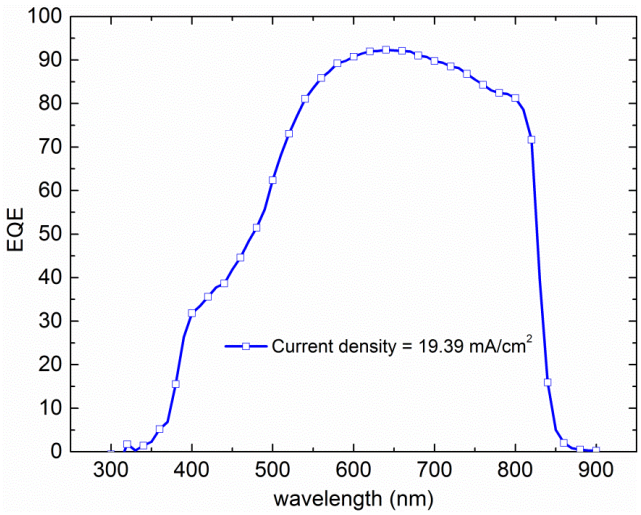

Figure 30. The external quantum efficiency (QE) for the highest efficiency device. The current density from QE is larger compared with that from J-V measurements. Table 11 shows the efficiency of the best performing device calculated from the current density as obtained from QE curve.

Table 11. Device performance parameters are tabulated for highest efficiency and highest open circuit voltage devices for CdTe solar cells in the substrate configuration. The efficiency for the highest efficiency device is also calculated based on the current density as measured from QE.

Performance Parameters			
Highest V_{oc} Device			
V_{oc} (V)	J_{sc} (mA/cm^2)	fill factor (%)	efficiency (%)
0.661	16.9	46.1	5.15
Highest Efficiency Device (Current Density from QE)			
V_{oc} (V)	J_{sc} (mA/cm^2)	fill factor (%)	efficiency (%)
0.606	19.4	52.4	6.86

I.2.2 Subtask 2: Fabrication of solar cells based on optimized downselected materials

The downselected materials will be used to fabricate solar cells. Novel contacts will be optimized based on heat treatment of the fabricated contacts. Substrate devices will also be fabricated and tested on the downselected materials.

Deliverables:

a. Comparative device performance results for superstrate-type solar cells using downselected novel contact materials and a description of process sensitivity for those devices. For example, device performance as a function of back contact deposition temperature.
b. Conditions for optimization of the back contact properties in superstrate-type solar cells as a function of heat treatments or other processing. For example, many contacts to Si require a heat treatment to produce the best contact. We will heat treat our novel contacts at temperatures from 100 to 500°C for 10 to 90 minutes to determine whether the contact improves. Microchemical, microstructural, and electronic characterization of the resulting devices will show the mechanism of any changes observed.
c. Best-effort solar cells based on the substrate geometry and using the novel contact materials. Evaluation to include alternate heterojunction partner materials and $CdCl_2$ heat treatment conditions for substrate-geometry devices.
d. Intensive efforts to disseminate the results to companies that could make use of the material both in photovoltaics and other applications as well as at least one publication each describing the optimized substrate and superstrate devices.

(a) University of Toledo Activities in Fabrication of CdTe Solar Cells with CIS:N Back Contacts in the Substrate Configuration

In spite of the relatively poor performance of the CdTe solar cells in the substrate configuration, studies have been undertaken using CIS:N back contacts in substrate type devices. The advantage is that a CIS:N substrate temperature of > 500°C can be used in the substrate configuration since the CIS:N is deposited before the CdTe/CdS solar cell. The substrates used for the CIS:N consist of borosilicate glass coated with sputtered Mo or a two layer structure of

sputtered Mo and atomic layer deposited MoO_3. The positive outome shown in Table 12 is that a significant improvement in performance has been achieved in the substrate configuration for 500°C vacuum-deposited CIS:N back contacts in comparison with 350°C vacuum-deposited

Table 12. Device performance parameters are tabulated for highest efficiency devices for CdTe solar cells in the substrate configuration without and with CIS:N back contacts. For the latter devices, the substrates were borosilicate glass coated with sputtered Mo (second entry) or a two layer structure of sputtered Mo and atomic layer deposited MoO_3 (third entry).

Cell Structure	V_{oc} (V)	J_{sc} (mA/cm^2)	Fill Factor (%)	Efficiency (%)
Substrate Solar Cell BSG/Mo/ CdTe/CdS/ZnO/ZnO:Al/grids	0.640	19.79	47.68	6.04
Best Substrate Solar Cell With CIS:N BSG/Mo/CIS:N/ CdTe/CdS/ZnO/ZnO:Al/grids	0.629	16.53	40.17	4.18
Best Substrate Solar Cell With MoO_3/CIS:N BSG/Mo/MoO_3/CIS:N/ CdTe/CdS/ZnO/ZnO:Al/grids	0.621	17.51	39.33	4.28

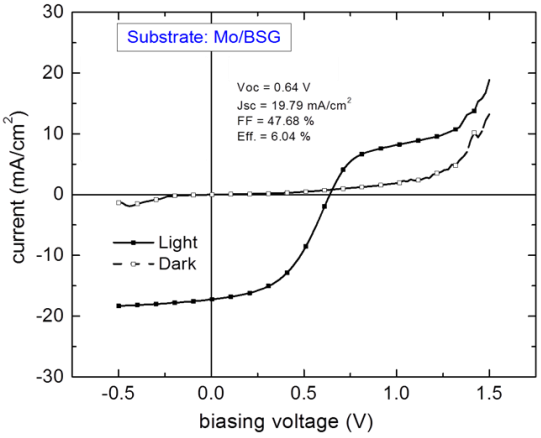

Figure 31. Light and dark J-V characteristics for a CdTe solar cell in the substrate configuration with a Mo back contact. The parameters are summarized as the first entry in Table 12.

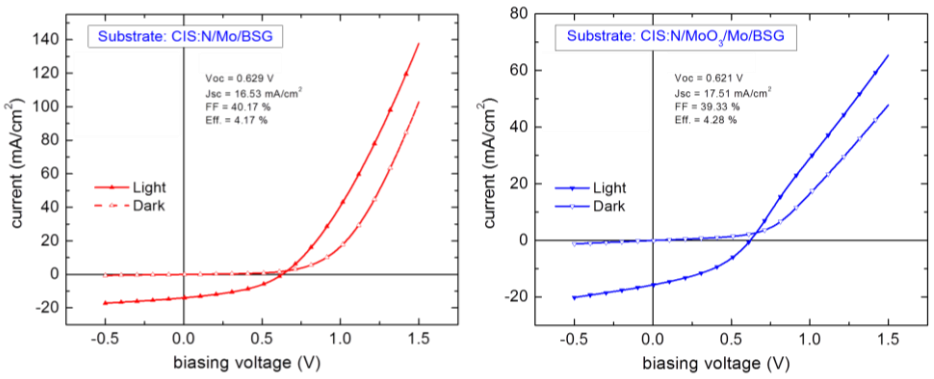

Figure 32. Light and dark J-V characteristics for CdTe solar cells in the substrate configuration with (left) Mo/CIS:N and Mo/MoO_3/CIS:N back contacts. The parameters are summarized as the second and third entries in Table 12.

CIS:N back contacts in the superstrate configuration, even with the much lower substrate cell baseline. In addition, the J-V characteristics appear to have improved compared to standard back contacts in the substrate configuration as shown in Figures 31 and 32. The efficiencies in Table 12 are lower, however, than cells fabricated in the superstrate configuration using spray-deposited CIS back contacts, and this may be affected by the lower substrate CdTe cell baseline.

Thus, in studies performed to date, the best CdTe solar cell with a chalcopyrite back contact was fabricated in the superstrate configuration with CIS deposited as a nanocrystalline film fabricated at low temperatures from liquid precursors. The open circuit voltage and fill-factor for this cell were 0.68 V and 48%, respectively. Greater success has been achieved thus far with Cu-free p-type pyrite back contacts prepared at room temperature from a nanocrystal solution. The highest performance cell with such a back contact exhibited an open circuit voltage of 0.81 V and a fill-factor of 69%. Further studies of pyrite incorporated into superstrate solar cells using different deposition procedures that incorporate Cu will be described next.

(b) University of Toledo Activities in Fabrication of CdTe Solar Cells with Nanocrystal Pyrite Back Contacts and Cu Incorporation in the Superstrate Configuration

For further studies of CdTe solar cells with nanocrystal pyrite back contacts, the CdS was layer of the cells was deposited by rf magnetron sputtering onto TEC-15/HRT (Pilkington N. A.) coated glass substrates. The CdTe absorber was prepared either by magnetron sputtering or by close space sublimation (CSS). For the standard back contact deposition in these studies, ~ 3 nm Cu and ~ 40 nm Au were evaporated thermally onto the $CdCl_2$-treated CdTe layer. The Cu was diffused into CdTe in an annealing step at 150 °C in dry air after Au deposition. For the novel

back contact, 3 nm Cu was thermally evaporated and diffused into the CdTe as for the standard contact, and a ~1 μm FeS_2 nanocrystal (NC) layer was deposited by drop-casting at room temperature in 1 atm N_2. The resulting FeS_2 NC are p-type semiconductors with high free carrier concentrations. The back contact was completed by evaporating ~40 nm Au onto the FeS_2 NC layer at room temperature. FeS_2 NC layers of varying thicknesses were explored while keeping other processing steps unchanged. Standard back contact cell areas (0.080 cm^2) were defined using a shadow mask during thermal evaporation; novel back contact cell areas (0.085 cm^2) were defined by mechanical or laser scribing. In these studies, QE measurements were found to confirm J_{SC} values. Current density vs. voltage measurements were performed in the dark, and under AM1.5G illumination.

Typical current density-voltage (J-V) curves for sputtered and CSS CdTe devices using two different back contacts are shown in Figure 33, and average parameters are shown in Table 13. In Figure 33, solid and dashed lines represent light and dark J-V curves, respectively. From the J-V curves in Figure 33 and the parameters values in Table 13, it is clear that adding an FeS_2 NC back contact layer improves the performance of the solar cells. Whereas J_{SC} appears similar for both back contact types, increases in V_{OC} and FF result in increased device efficiency when using the Cu/FeS_2/Au back contact. The increases in V_{OC} and FF are observed in both sputtered and CSS CdTe devices; in fact, V_{OC} has increased by ~2% and ~3%, respectively. Solar cell parameters shown in Table 13 represent an average of 20 cells for the Cu/Au back contacts and an average of 28 cells for the Cu/FeS_2-NC/Au back contacts.

Incorporation of 3 nm Cu appears between the CdTe and FeS_2 appears to reduce any residual back barrier width and thus improves the hole collection efficiency. These results suggest that a heavily-doped semiconductor layer between the CdTe and metallic layers can, with suitable band edge alignments, improve the performance of CdTe solar cells by promoting hole flow from the CdTe into the back contact metal. Requirements for the intermediate semiconductor layer are that it be p-type in nature with high carrier density (~10^{18}-10^{19} cm^{-3}) and with a valence band offset between the CdTe and interface layer that is very small. Although not yet investigated

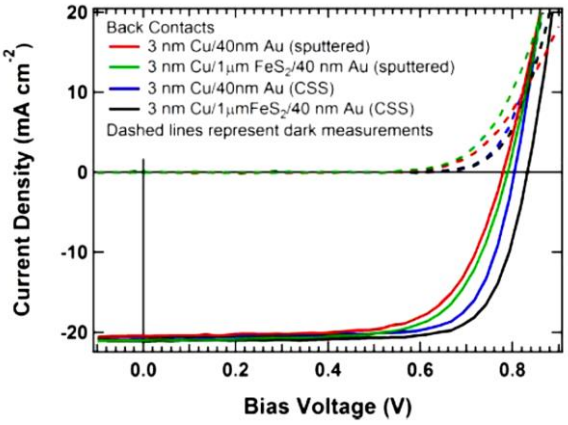

Figure 33. Current voltage characteristics for sputtered and CSS CdTe solar cells using two different back contacts. Approximate thickness of each back contact layer is given.

Table 13. Average performance parameters for CdTe solar cells using two different back contacts for sputtered and CSS deposited absorbers. Averages were taken from 20 cells for Cu/Au back contacts and from 28 cells for Cu/FeS_2/Au back contacts.

Sputtered CdS/CdTe						
Back Contact Type	**V_{OC} (V)**	**J_{SC} (mA cm^{-2})**	**FF (%)**	**η (%)**	**R_S (Ω cm^2)**	**R_{Sh} (Ω cm^2)**
Cu/Au (20)	0.778 ± 0.02	20.5 ± 0.3	68.3 ± 1.7	10.9 ± 0.5	4.1 ± 0.6	2219 ± 355
Cu/FeS_2/Au (28)	0.792 ± 0.01	20.9 ± 0.8	68.6 ± 2.0	11.4 ± 0.7	4.0 ± 1.4	2744 ± 1024
Sputtered CdS / CSS CdTe						
Cu/Au (20)	0.809 ± 0.008	21.0 ± 0.3	74.7 ± 1.1	12.7 ± 0.1	2.6 ± 0.7	2947 ± 976
Cu/FeS_2/Au (28)	0.835 ± 0.003	21.3 ± 0.4	75.0 ± 0.9	13.4 ± 0.3	2.9 ± 1.0	4839 ± 2781

experimentally in detail, it has been proposed that the NC-FeS_2 forms an ohmic contact to Au, and that the FeS_2/CdTe junction shows a valence band offset favoring efficient hole transfer.

A thick layer of FeS_2 NC is used in this study to reduce pin-holes present in FeS_2 films. Thus, a thick layer of NC film passivates any shunting pathways from the back contact, which is also clear from the observed higher shunt resistance. Current-voltage characteristics of CdS/CdTe devices incorporating FeS_2 NC layers of varying thicknesses are shown in Figure 34 and their J-V parameters are shown in Table 14. This study shows that the performance is essentially independent of the thickness as long as the FeS_2 NC layer is ~1μm or thicker. Typical EQE spectra of CdTe devices with and without the FeS_2 NC layer are shown Figure 35 where a blue-shift by 5 to 10 nm can be noted in the band gap collection cut-off for the cell with the FeS_2 NC layer. Further investigation of this effect is warranted.

This work illustrates the application of nanocrystalline iron pyrite as a back contact layer between Cu and Au depositions to improve the CdS/CdTe solar cell performance. Using FeS_2 in this back contact structure has led to an increased CdS/CdTe device efficiency by ~ 9% relative to the standard back contact. Experimental results indicate that the FeS_2 NC layer may serve as a substitute for ZnTe, which has alse been used in similar applications. Undoped ZnTe has very low carrier density (~10^{15} cm^{-3}) and thus ZnTe must be doped before using it as a back contact interface layer. Cu doping of ZnTe initially improves the performance but diffusion of Cu may degrade it ultimately. Since the carrier density of FeS_2 is already very high through native defects, doping is unnecessary which affords simplicity and avoids additional Cu within the device. The disadvantage of the FeS_2-NC layer fabricated by the LbL method, however, is that a hydrazine treatment is required to remove the NC surfactant molecules in order to improve the conductivity of the film. Thus, although the FeS_2 is an earth abundant, nontoxic sulfide, the NC method is not generally considered economically viable for large scale production due to the concerns over the volatility and toxicity of hydrazine. In the next section, the development and demonstration of a hybrid vacuum deposition method for depositing polycrystalline iron pyrite thin films on CdTe are described. This vacuum deposition method avoids the use of hydrazine and so may be of greater interest to industry in large scale production.

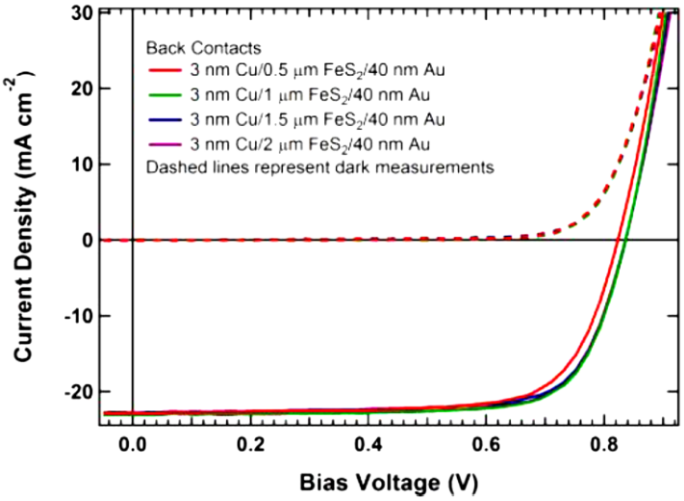

Figure 34. The thickness dependence of the J-V behavior for an FeS_2 NC back contact layer; the thicknesses of the Cu and Au layers were held constant. The performance parameters of these cells are shown in Table 14.

Table 14. Performance parameters of the best cells obtained for FeS_2 NC back contacts with thicknesses ranging from 0.5 μm to 2 μm; the thicknesses of the Cu and Au were maintained constant.

Back Contacts Cu = 3nm, Au = 40 nm	V_{OC} (V)	J_{SC} (mA cm^{-2})	FF (%)	η (%)
Cu/0.5μm FeS_2/Au	0.824	23.1	73.0	13.9
Cu/1μm FeS_2/Au	0.836	22.9	75.2	14.4
Cu/1.5μm FeS_2/Au	0.837	22.9	74.2	14.2
Cu/2μm FeS_2/Au	0.836	23.0	74.7	14.4

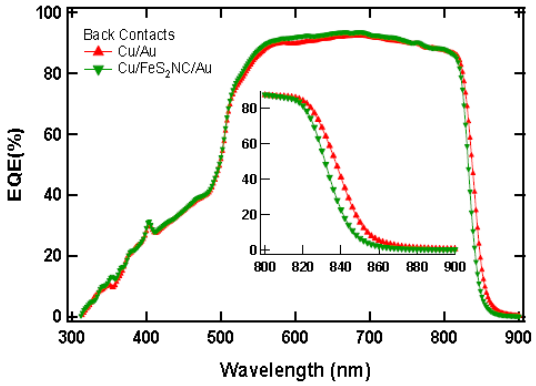

Figure 35. Typical external quantum efficiency (EQE) of cells before and after incorporation of FeS_2 NC as an interface layer for CSS deposited CdTe devices. The inset provides an expanded view in the CdTe bandgap region.

(c) University of Toledo Activities in Fabrication of CdTe Solar Cells with Hybrid Deposited Thin Film Pyrite Back Contacts with Cu Incorporation in the Superstrate Configuration

The high free hole (p+) density and the relatively deep work function (~5 eV) exhibited by FeS_2 nanocrystal films support these materials as candidates for low-resistance back contacts in CdS/CdTe solar cells. Initial promising results were obtained applying solution processing based on colloidal FeS_2 nanocrystals (NCs), deposited and chemically modified using hydrazine to improve the conductivity. These results demonstrated an improvement in solar conversion efficiency of at least 5% when compared with test cells incorporating laboratory standard Cu/Au back contacts. Since the cubic FeS_2 NCs have an average edge length of ~100 nm, thin films prepared with this material are porous. To minimize the adverse effects of porosity of the FeS_2 NC film at the CdTe back contact, an FeS_2-NC film of ~1.0 μm thickness is required to enhance the performance of the solar cells. In addition, when preparing the FeS_2-NC films by the solution methods, treatment by hydrazine is applied to remove the NC surfactant molecules and improve the conductivity. The use of hydrazine is undesirable for large-scale processing by

industry due to concerns of its volatility and toxicity. Motivated by these issues, a hybrid vacuum deposition method was developed and optimized for making polycrystalline iron pyrite thin films on CdTe. This method relies on sputtering iron and concurrently evaporating sulfur to form a back contact on the CdS/CdTe film-stack, while maintining the temperature of the stack below 400°C to avoid modifying the underlying cell via CdTe evaporation. Our investigations have revealed favorable results, with CdS/CdTe/FeS_2 devices showing improvements in the open circuit voltage (V_{OC}), fill-factor (FF), and the power conversion efficiency under AM1.5G simulated solar illumination**.**

Cadmium sulfide (CdS) and CdTe layers were deposited by RF magnetron sputtering onto TEC-15/HRT glass substrates (Pilkington N.A.). The thicknesses of CdS and CdTe films used in this study were ~ 80 nm and ~2 μm respectively. For characterization purposes, polycrystalline iron pyrite (FeS_2) films were prepared on soda lime glass and silicon wafers for structural and optical characterization. In addition, FeS_2 was deposited onto the $CdCl_2$-treated CdTe layers of CdS/CdTe solar cells for completion into working PV devices. These cells were completed by evaporation of Cu/Au metal layers, followed by thermal treatment to enhance the diffusion of Cu into the CdTe/FeS_2 filmstack. The FeS_2 films were prepared by hybrid DC sputtering of iron with co-evaporation of elemental sulfur. The FeS_2 film was deposited at 300°C substrate temperature, 4 mTorr Ar pressure, and 70 W DC sputtering power. Another important parameter found to determine crystalline properties of the iron sulfide was the sulfur evaporation rate (SER). Several SER values were investigated, and high quality iron pyrite was obtained when the SER was within the range of ~ 0.2 nm/s to ~ 0.4 nm/s. The deposition time was varied from 5 to 60 minutes which produced films of thickness from ~30 nm to ~750 nm, depending also on the selected SER.

The crystal structure of FeS_2 films deposited on soda lime glass and silicon wafers was determined by X-ray diffraction spectroscopy (XRD) and Raman spectroscopy measurements; surface morphology was determined using scanning electron microscopy (SEM); and material composition was measured using energy dispersive X-ray (EDX) spectroscopy. The hybrid-deposited FeS_2 films have the same cubic crystal structure and pyrite phase, but according to the peak intensity of XRD spectra, the films appear smaller-grained crystalline compared to the previously studied FeS_2-NC films. This may be due to the relatively low substrate temperature (< 400 °C) which yields a high crystallite nucleation density. Several substrate temperatures were evaluated starting from 200 °C to 350 °C, and it was found that pure iron pyrite phase FeS_2 was obtained at an optimum of 300°C. The lattice constant was calculated from the various FeS_2 films deposited at 300 °C and found to be 0.5423 nm. Scanning electron microscopy (SEM) showed that the average grain size of hybrid deposited FeS_2 is smaller than the size of NCs. The average atomic percentage of S to Fe was found to be 2.08 when the substrate temperature was 300 °C, but the ratio was higher when the film was fabricated at lower substrate temperatures. Hall measurements indicated that the FeS_2 film is p-type with carrier density of the order of 10^{20}

cm^{-3} and mobility of ~ 8 cm^2/Vs. Higher mobility is expected to be beneficial for improved back contact performance.

When an FeS_2 film was deposited as the interface layer for CdS/CdTe solar cells, film thicknesses of < 100 nm were preferred for high performance. Although a complete study of the dependence of device performance on FeS_2 film thickness study has not yet been undertaken, a reduced thickness is desired as it reduces (i) the deposition time, (ii) the required amount of Cu deposited at the surface of the FeS_2 in this case, and (iii) the time and temperature required for Cu diffusion during processing. For the standard back contact deposition, ~3 nm Cu and ~40 nm Au are thermally evaporated, sequentially, onto the $CdCl_2$-treated CdTe layer. Subsequently, Cu is diffused into the CdTe by annealing at 150 °C in dry air. The identical Cu/Au evaporation and thermally-driven diffusion steps were followed to complete metal back contact on top of the thin FeS_2 back contact film fabricated on CdTe. For both standard and novel back contacts, the cell areas (0.085 cm^2) were defined by laser scribing. Quantum efficiency (QE) measurements were used to confirm J_{SC} values. Current density vs. voltage measurements were performed in the dark, and under 1 Sun AM1.5G illumination. These curves for the best device using each of the two back contact designs are shown in Figure 35. In this figure, solid lines represent the light J-V measurements and dashed lines represent the dark measurements. The average J-V characteristic parameters for 20 devices prepared for each type of contact are shown in Table 15. From the J-V curves shown in Figure 35 and the parameter values in Table 15, it can be seen that adding a thin layer of FeS_2 as an interface layer has improved the device performance. While the J_{SC} appears similar for both back contact types, increases in V_{OC} and FF result in increased device efficiency when using the FeS_2/Cu/Au back contact. The relative increase in V_{OC} is more than 2% and the relative increase in FF is 8% for the CdTe solar cells shown in Figure 35.

The improvement in device performance observed here for the hybrid deposition process for FeS_2 approximately reproduces the improvement seen when using FeS_2-NC as a back contact interface layer. In addition to the significantly different method of FeS_2 preparation (solution processing vs. hybrid sputtering/co-evaporation), the results reported for hybrid deposition are obtained by introducing the Cu at a different point in the process. In the case of the solution-processed FeS_2 contact layer, Cu is introduced and diffused into the CdTe *prior to* deposition of the FeS_2-NC and evaporated Au layers (no thermal processing is used during or subsequent to the FeS_2-NC/Au processing). Generally poor performance was found, however, for devices prepared with Cu prior to the hybrid vacuum deposition of FeS_2. This is attributed to excessive diffusion of Cu associated with the elevated substrate temperature present during vacuum deposition of the FeS_2. Therefore, the hybrid sputtered/co-evaporated thin film of FeS_2 is first deposited onto the CdTe surface, and the device is then completed by evaporation of Cu/Au and subsequently annealing the device to enhance Cu diffusion.

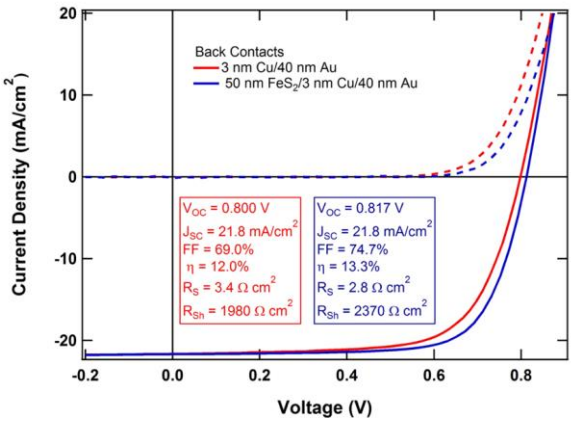

Figure 35. Current voltage characteristics for sputtered CdTe solar cells using standard and hybrid deposited FeS_2 back contacts; the approximate thicknesses of each back contact type are shown in the graph. J_{SC} was verified by using external quantum efficiency.

In comparison with the FeS_2-NC film, the FeS_2 film prepared by using the sputtered/ co-evaporated method is more uniform and compact and the film strongly adheres to the substrate. Due to the improved FeS_2 film density, CdTe devices using a sub-100 nm thick hybrid-deposited back contacts perform at a level equal to the performance of devices utilizing a ~1 μm thick FeS_2-NC back contact. Typical external quantum efficiency (EQE) curves of CdTe devices with and without the FeS_2 interface layer are shown in Figure 36. The EQE spectra show that current collection improves slightly in the wavelength range of ~700 nm to 860 nm. It is concluded that electron-hole pairs generated away from the CdS/CdTe p-n junction, due principally to these long wavelength photons, benefit from the lower barrier potential present within the CdTe/FeS_2/Cu/Au contact. Since the Cu is deposited and diffused after FeS_2 deposition, the conductivities of both FeS_2 and CdTe films may have increased as a result. There is no blue shift, however, in the band edge behavior for thin film FeS_2 back contact layer as in the case of FeS_2-NC, another positive outcome.

Table 15. Average parameters of CdTe solar cells prepared using using standard and hybrid deposited FeS_2 back contacts for sputtered CdTe solar cells; average values were calculated for 20 cells of each contact type. J_{SC} values are those obtained from the J-V measurement system.

Back Contact Type	V_{OC} (V)	J_{SC} (mA cm^{-2})	FF (%)	η (%)	R_S (Ω cm^2)	R_{Sh} (Ω cm^2)
Cu/Au (20)	0.793 ± 0.010	21.7 ± 0.2	68.4 ± 0.9	11.8 ± 0.2	3.7 ± 0.4	1619 ± 212
FeS_2/Cu/Au (20)	0.812 ± 0.002	21.4 ± 0.3	72.8 ± 0.9	12.7 ± 0.3	3.1 ± 0.3	2580 ± 556

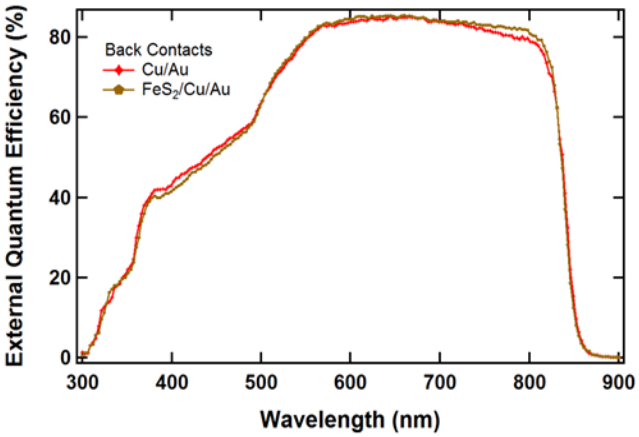

Figure 36. Typical external quantum efficiency of cells with and without FeS_2 as a back contact interface layer for CdTe solar cells.

In summary, this work demonstrates the application of a hybrid sputter/co-evaporation method for preparing thin film iron pyrite as the interface layer at the back contact of CdS/CdTe solar cells. Initial results indicate that devices including a pyrite FeS_2 back contact layer perform well, showing improvements in V_{OC}, FF, and PCE as compared with a standard Cu/Au contact. The FeS_2 back contact may ultimately benefit from further optimization to attain increased CdTe solar cell efficiency. Open-circuit light soak tests are underway to test the stability of the modified back contact design, and collaboration with U.S. industry is planned for further evaluation of these back contact structures.

I.2.3 Subtask 3: Testing and modeling of solar cells.

The optimized solar cells will be tested and the results modeled to quantitatively determine the performance of the novel contact materials.

Deliverables:

a. Temperature-dependent light and dark current/voltage, capacitance/voltage and other measurements of the solar cells produced above.
b. Modeling and analysis of the data and determination of Schottky barrier heights and diode properties including built-in voltage.
c. Preparation of an abstract describing the results of the work submitted to the 2014 and/or 2015 IEEE Photovoltaic Specialists Conferences.

I.2.4 Subtask 4: Stability testing.

The stability of the optimized downselected materials in both substrate and superstrate configurations will be examined using both standard accelerated lifetime test conditions and more aggressive annealing.

Deliverables

a. Results of standard accelerated lifetime testing to evaluate the stability of all active devices produced with novel contact materials along with stability tests on baseline cells.
b. Results of annealing studies including device performance as a function of anneal temperatures and times and microstructural and microchemical analyses to determine reactions or interdiffusion mechanisms resulting in device degradation or failure.

(a) University of Toledo Studies of the Stability of Thin Film Pyrite Back Contacts

A potential concern is the diffusion of Fe from the FeS_2 back contact into the CdTe which would be expected to degrade the cell performance. Figure 37 shows promising results for the stability of such back contact layers. In this figure, J-V characteristics of a CdTe solar cell with a sputtered absorber layer and a 1 μm thick FeS_2–NC layer are measured after exposure to a N_2 environment at 100°C for 23 hours, and at 200°C for one additional hour. Very little degradation is observed during this annealing process. Open-circuit light soak testing was also performed to understand the stability of different back contact designs. It was found that devices with back contact of Cu/FeS_2-NC/Au are more stable comparable to the standard Cu/Au back contact. Future studies of vacuum deposited FeS_2 back contact structures containing Cu are needed, and these will be done in conjunction with future industrial collaborations.

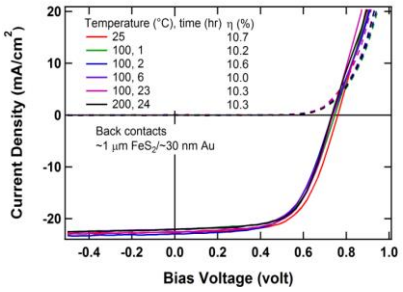

Figure 37. Stability of a CdTe solar cell with a sputtered absorber layer and a 1 μm FeS_2 back contact as measured under N_2 at 100°C for 23 hours, and at 200°C for one additional hour.

(a) University of Illinois Studies of the Properties of Grains and Grain Boundaries in CdTe

To clarify the nature of contacts to CdTe, we have studied the properties of grain boundaries and grains by cathodoluminescence and scanning microwave impedance microscopy. Samples were the same CdTe devices produced at the University of Toledo grown by rf-sputtering as described above with and without back contacts. The photoluminescence measurement showed subgap emissions associated defect states at low excitation powers and with excitons at higher excitation powers. We looked at the effect of Cu on these emissions by deposition (at Toledo) of Cu onto the back of the device following the same procedure as normally used in the device fabrication.

This study extended the previous works providing a more detailed characterization of the temperature and power dependence of luminescence peaks. Results agree with the spectra obtained from materials produced by thermal evaporation. Thus, we expect that the results are relevant to other materials than those produced by sputtering. One of the more remarkable results obtained was that Cu doping suppressed the sub-gap luminescence, resulting in increased band-to-band recombination. The reduced recombination via defects suggests an explanation for the increased open-circuit voltage in CdTe devices treated with Cu.

For the studies reported here the devices were complete except for the addition of contacts including a $CdCl_2$ treatment, described above. Two different treatments were used to complete the cells. One sample (sample A) had a bare CdTe back surface while a second sample (sample B) included deposition of 3 nm Cu/30 nm Au bilayer contacts. Sample B was subsequently annealed at 150^o C in air for 45 min to activate the contacts. Both samples (A and B) were 1 cm x 1 cm devices. Sample B $V_{oc} \sim 0.8$ V, $J_{SC} \sim 22$ mA/cm^2, and an efficiency of ~12%.

For PL studies the samples were mounted on a temperature-controlled vacuum cryostage. Each sample was cooled to 85K using liquid nitrogen and reheated with a resistive heater to a controlled temperature between 85 and 295 K. The samples were illuminated using a 532 nm Nd:YAG laser with a peak power of <50 mW and a maximum average laser power of ~11 mW. The laser spot size was ~0.2 mm^2, resulting in a power density of 5.5 W/cm^2. The power was reduced as needed using neutral density filters rather than by reduction of the laser power. A Princeton Instruments Spectra-Pro 300i grating monochromator and a PIXIS 100 Si CCD detector collected and analyzed the emitted light. Some measurements were made through the front (glass side) of the device to compare the CdTe near the junction with the CdTe near the back contact. For measurements through the CdS, ~6% of the 532 nm laser light was absorbed in the CdS. We further estimate that ~50% of the light was absorbed in the first 100 nm of the CdTe near the heterojunction. Therefore we anticipate that the majority of the data from measurements through the CdS represents carriers generated within 100 nm of the junction, while measurements from the rear of the CdTe represent the behavior of carriers generated within a similar distance of the back surface. Only Sample A was studied from the back surface

of the CdTe due to the contact metal present on the rear of Sample B, while both were measured through the glass side.

The results of this study are summarized in Figure 38 for measurements through the back CdTe surface of Sample A, in Figure 39 for Sample A through the glass, and in Figure 40 for Sample B (Cu/Au on the rear) excited through the glass. For all three samples the spectra show two main components, one broad band between 1.42 and 1.52 eV and a second emission near the bandgap at ~1.55 eV. The broad low energy emissions dominate at lower excitation power and at low temperature where carriers are most likely to be trapped in defect states. Both samples measured through the glass show much greater band-to-band (1.55 eV) emissions than for the data for Sample A measured from the rear of the device.

In all three measurements the behavior of the long wavelength emissions is consistent with a free-to-bound type of transition. The intensity of the resulting emissions scales as a power of the excitation intensity with the exponent being ~0.6 for Sample A measured from the rear and 0.8 to 0.9 for samples A and B, respectively, measured from the front of the device. These emissions show a thermally-activated quenching behavior with an activation energy of ~100 mV. Previous studies of photoluminescence from CdTe and device quality CdS/CdTe heterojunctions reported similar peaks. The low energy emission band has been associated with transitions involving a Cl_{Te}-V_{Cd} defect complex.

By contrast the emissions at 1.55 eV scale with illumination intensity with exponents of ~2, consistent with an excitonic transition, as one would expect for a band-to-band transition. Temperature dependence of the energy gap was observed for all results. The absence of a significant shift in the near band edge emissions when measured near the junction indicates that this emission is not affected by grading of the material near the heterojunction. The band edge emission is due to bound excitons.

The similarity of the behavior of the various components and measurements indicates that these emissions are associated with excitons bound to the same impurity/defect. Acceptor-bound excitons have been observed previously in PL spectra of CdTe where the acceptor was proposed to be the V_{Cd}-Cl_{Te} defect complex. When the Cu/Au back contact is added the band-to-band bound exciton shifted up by 10 meV as might be expected if this peak is due to an acceptor bound exciton. In this case Cu_{Cd} should be the primary acceptor and the corresponding emission energy should be increased.

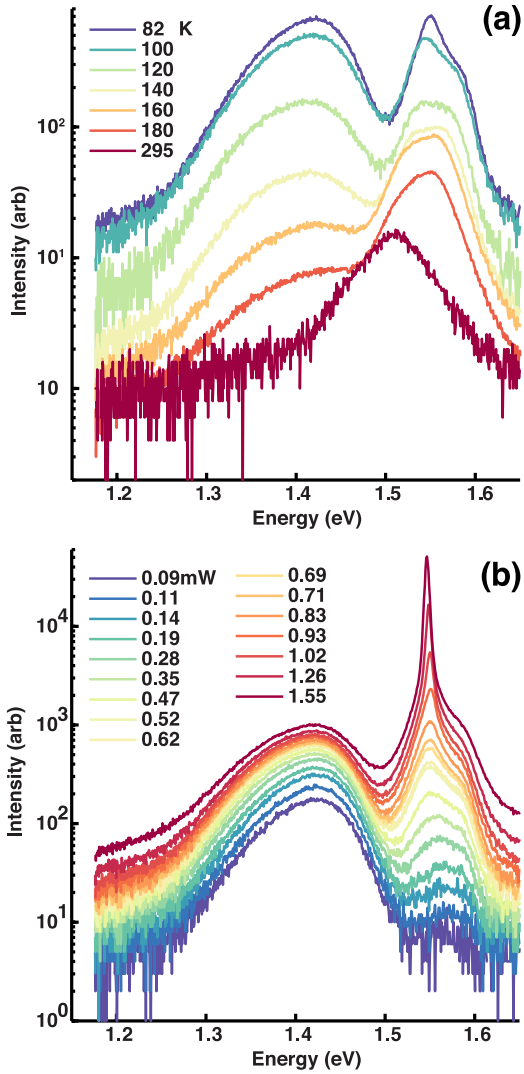

Figure 38: PL spectra measured through the rear side of Sample A at (a) ~0.7 mW laser power over a range of temperatures and (b) at 82 K for various laser powers.

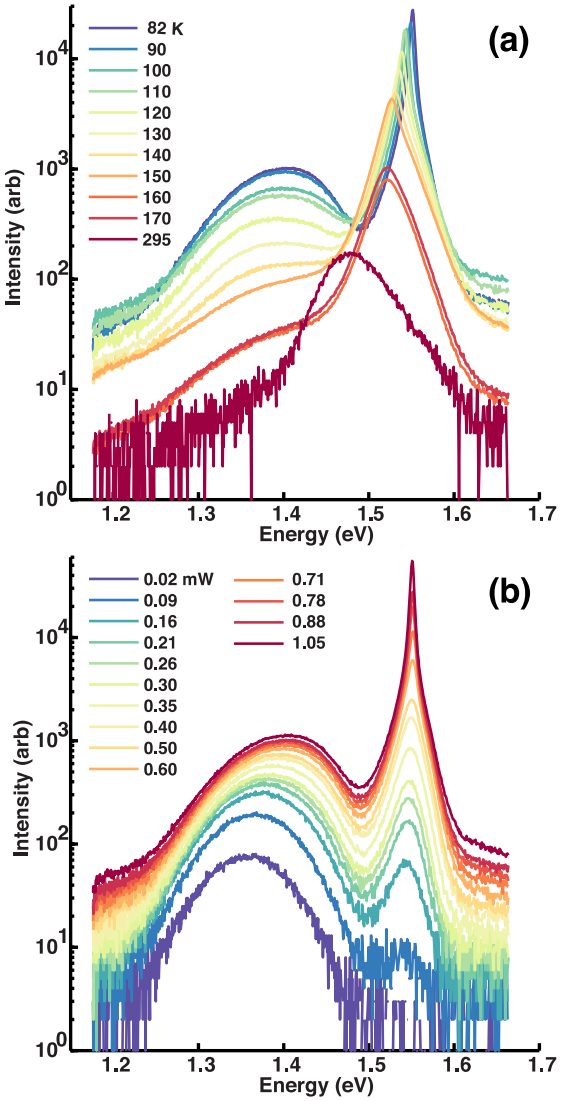

Figure 39: PL spectra for Sample A measured through the glass (front junction) side at (a) ~0.9 mW laser excitation power over a range of temperatures and (b) at 82 K as a function of laser power.

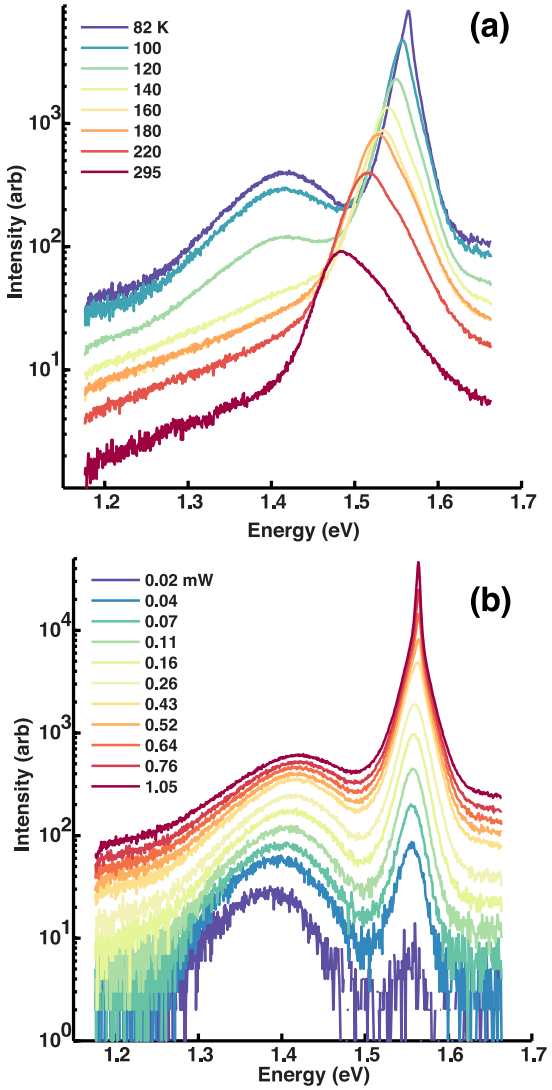

Figure 40: PL spectra obtained for Sample B (with Cu) through the glass (front junction side) at (a) 0.5 mW laser power as a function of measurement temperature and (b) at 82 K as a function of laser excitation power.

Addition of Cu back contacts was found to suppress the sub-bandgap emissions, especially for the measurements near the heterojunction even though the Cu was present only at the back surface of the device. At the same time, when Cu was added to the material (Sample B) the band-to-band transitions dominated the spectra at all excitation powers. We anticipate that this is the result of extended lifetimes for trapped minority carriers in the defects associated with the free-to-bound transitions. We interpret the results as follows. We suggest that the Cu was incorporated as interstitials (Cu_i) that diffuses rapidly during contact activation, forming Cu_i-V_{Cd} acceptor complexes, Cu on V_{Cd} (Cu_{Cd}) acceptors and Cu_{Cd}-Cu_i neutral complexes. This may disrupt the Cl_{Te}-V_{Cd} acceptor complexes that give rise to the low energy emissions. This explains the reduction in free-to-bound transitions compared to the Sample A results. Romero et al. proposed that Cu_{Cd} acceptors are exceptionally effective recombination centers. We therefore expect that the free-to-bound transitions in Sample B involve the Cu_{Cd} defects.

We conclude that the PL spectra reported here and those observed by others show that the sputtered CdTe behaves the same way as materials deposited by evaporation. This work was published in *Journal of Materials Research*, v 31, n 2, p 186-194, January 6, 2016.

The effect of $CdCl_2$ treatment on the properties of grain boundaries in CdTe was studied by scanning microwave impedance microscopy (sMIM). sMIM is a high-resolution scanning probe-based technique, capable of measuring conductivity and dielectric constant of a semiconductor surface based on near-field microwave reflectivity modifying the tuning of a transmission line. With sMIM one can map material permittivity and conductance with high signal-to-noise ratio, a lateral resolution related to the scanning tip size and a depth resolution limited by the skin depth of the sample at the microwave frequency. The technique relies on reflection of microwaves applied to the sample surface through the shielded conductive AFM tip that is scanned across the surface. In the current experiments, a low power (-5 dBm), ~3 GHz rf signal was used and the in-phase and out-of phase components of the reflected power were used to determine the local permittivity (capacitance) and conductivity (resistance) of the sample. The measurement technique was calibrated using purely capacitive Al_2O_3 dots on SiO_2/Si substrates to obtain the signature of a capacitive response, which allowed separation of the resistive component. Both could be mapped and displayed independently. The sMIM measurements were performed using an Asylum Research MFP-3D AFM and cantilevers from PrimeNano Inc. All measurements were performed in contact mode.

Initial measurements clearly showed that the raw capacitance and conductivity data was strongly influenced by the area of interaction between the sample and tip, which was related in turn to surface morphology. To remove the effect of surface morphology we applied an intermediate frequency (~250 kHz) ac bias to the scanning tip and used a lock-in amplifier to extract the dC/dV behavior of the sample. The ac signal amplitude was 2V peak-to-peak for all measurements reported here. Comparison of the dC/dV results with the surface morphology measured by the scanning probe height data shows that this approach completely removes the effect of surface morphology from the data. It was found that the signal-to-noise of the data was

significantly improved by deposition of ~5 nm of Al_2O_3 by atomic layer deposition across the sample surface. Therefore all data presented here had such an Al_2O_3 layer added. In addition, a dc bias could be included on the probe tip to cause accumulation or depletion of majority carriers under the tip. We note that because the sign of the dc bias determines the type of carrier that accumulates under the tip, we can determine the majority carrier type by this method. This can also be determined from the sign of the phase angle of the dC/dV data. A schematic diagram of the apparatus used for sMIM measurements is presented in Figure 41.

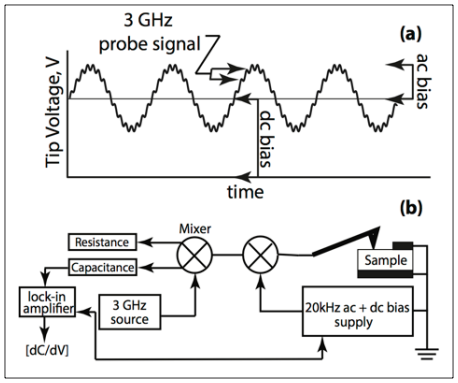

Figure 41: a schematic diagram for the sMIM measurement system used here.

To keep the tip bias exclusive of one polarity, the dc bias was adjusted such that the ac signal did not reverse the tip bias during any portion of the cycle unless the dc bias was zero, hence the ac signal was symmetric about ground.

By changing the dc bias on the tip and determining the capacitance of the sample locally, it was possible as well to determine an effective capacitance/voltage curve for the sample with ~50 nm resolution. In some similar measurements by a technique referred to as scanning capacitance microscopy (SCM), the tip is grounded and a bias is applied to the sample. This means that the behaviors measured are a convolution of the tip-surface capacitance and the junction capacitance. Furthermore the signal-to-noise ratio of SCM is not as good as sMIM. For all

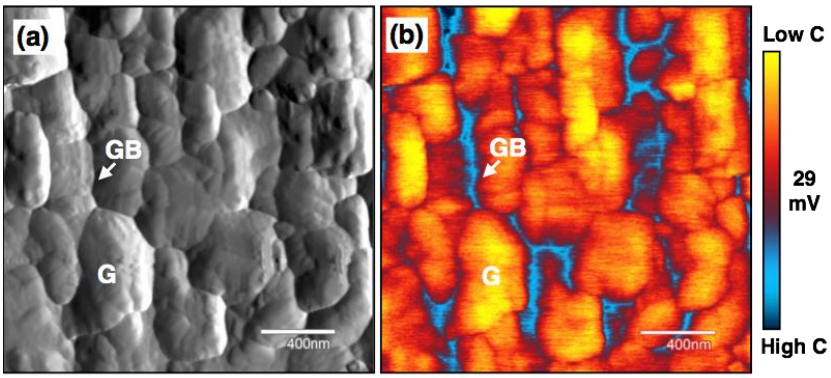

Figure 42: (a) deflection (derivative of height) and (b) capacitance data for a CdTe device measured near the back contact. There is a clear correlation between topography and

measurements described here, both contacts to the sample were grounded so there was no voltage or photovoltage across the device. All biases were applied through the tip.

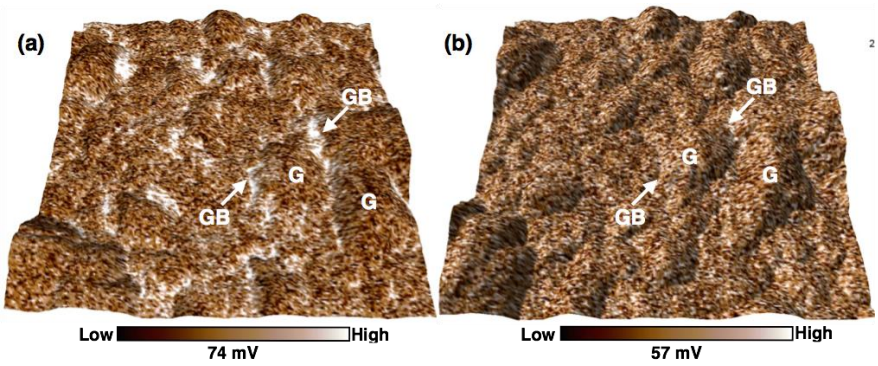

Figure 43: shows the behavior of the sample tip under (a) +2V bias and (b) -2V bias.

Figure 42 shows the deflection (dz/dx) and capacitance (C) data for the surface of a CdTe device near the back contact. Clearly there is a strong correlation between the height data and the capacitance data. However, measuring dC/dV yields a very different result. In Figure 43 we show the behavior for a +2 and -2V dc bias on the tip. In this figure the capacitance data in brown has been overlain on the topography data. The capacitance data shows little effect of topography but clearly shows an increase in capacitance in the grain boundaries. This is consistent with a depletion of carrier concentration at those locations. By analysis of the phase of the microwave signal we further determined that there is no change in majority carrier type in the grain boundaries, hence simple depletion of p-type carriers is occurring. Applying a -2 V bias to the tip causes elimination of the contrast between grains and grain boundaries,

presumably due to enhancement of majority carriers in the grains by application of tip bias. Note that the capacitance is reduced across the image when the tip bias is reversed.

One of the most interesting observations based on this work to date is the measurement of the effect of light on the sample. We do not have a high performance lamp on the sample but we have measured the difference in behavior of a sample with the illuminator lamp for the AFM on and off and compared the results. The data is shown in Figure 44. There is an enhancement in the capacitance in the grain boundaries when the illuminator was on.

We have extended the above results at the end of the project to specifically measure the effect of $CdCl_2$ on CdTe devices. For this work we have also compared samples deposited by closed space sublimation (CSS) from the University of South Florida group lead by Ferekides with samples described above from Toledo.

The deposition process for the CSS samples has been described in detail elsewhere. The substrate was Corning EagleXG glass coated with sputtered indium tin oxide (ITO) as the front contact. CdS and CdTe were deposited sequentially by chemical bath deposition (CBD) and CSS, respectively. The CSS substrate temperature was 550− 600 ° C and the source temperatures

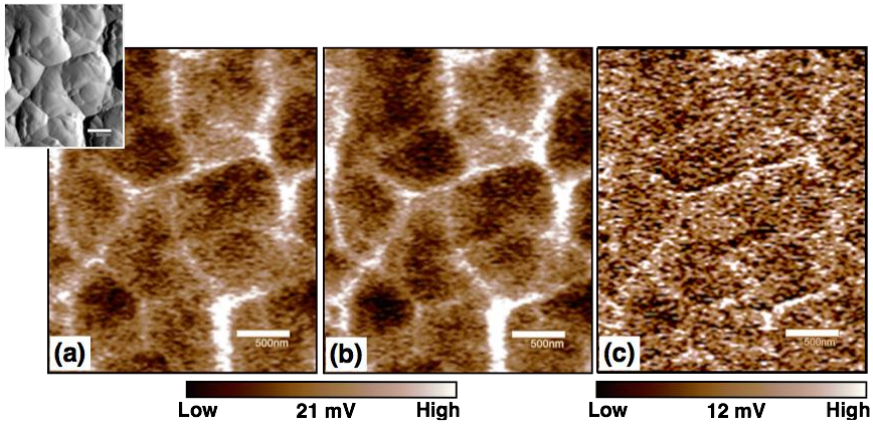

Figure 44: dC/dV data for a CdTe device sample measured with the illuminator (a) off and (b) on and (c) the difference in the two scans. The sample topography is shown in the insert.

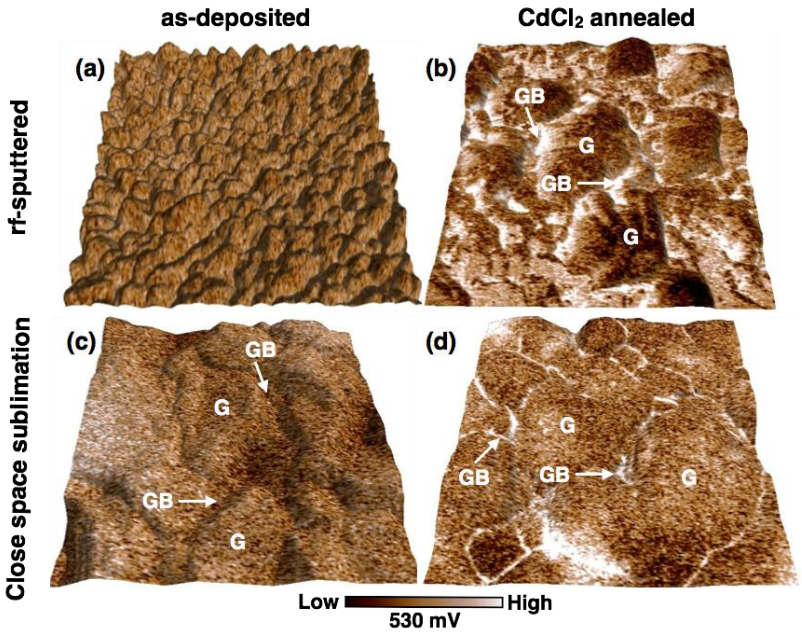

Figure 45: sMIM dC/dV data for four samples, two rf sputtered from the University of Toledo and two closed space sublimated (CSS) from the University of South Florida. The left two samples (a) and (c) are as deposited while the two images to the right are for $CdCl_2$ treated were 650− 680 ° C. Samples before and after $CdCl_2$ treatment were prepared. The $CdCl_2$ was deposited by evaporation and annealed in 80% He, 20% O_2 at 400 ° C for 30 min. Devices produced by this method typically show V_{oc} ~800-850 mV, J_{sc} ~20-23 mA/cm^2, FF ~ 70−75%, and efficiency ~11−15%.

The results of the sMIM analysis are shown in Figure 45. Both samples show relatively little change in grain boundary response compared to the bulk grains. This indicates that as-grown material has little potential associated with grain boundaries in CdTe. By contrast, in $CdCl_2$ treated samples from both groups there is clear indication of increased capacitance response, suggesting grain boundary depletion. The CSS film shows little grain growth during $CdCl_2$ treatment, while the sputtered material shows dramatically larger grains. Thus, the grain boundary depletion is not directly connected to grain growth. Reduction in carrier concentration at grain boundaries would result in collection of minority carriers there. However, the low carrier concentration would also suggest a relatively low recombination rate (low np product), which may explain why grain boundaries in the $CdCl_2$-treated material are not harmful. We attribute the grain boundary depletion to the presence of Cl in the boundaries as Cl on a Te site would be a donor. However, other structural changes in the grain boundaries could account for

the change in carrier concentrations. We further note that the phase angle measured for these materials is too small to represent a change in majority carrier type. Therefore, we conclude that the grain boundaries are not inverted (n-type).

The results of sMIM analysis of the effects of $CdCl_2$ treatment on CdTe have been published in J. Phys. Chem C, 2016 in press (DoI: 10.1021/acs.jpcc.6b00874).

Task #3 – *Evaluation of the potential of the materials developed in the project*

> A final analysis of the materials studied, their potential as contacts to CdTe solar cells in competition with other candidate materials, progress toward commercialization of the materials, and any broader applications will be detailed in a final report and publication.

We have examined a wide range of materials as contacts to CdTe. The overall conclusions of the project are as follows:

1) Doping CIGS p-type: we have shown that we can dope CIGS p-type with nitrogen over a range of compositions resulting in up to six orders of magnitude increase in conductivity. For heavy N doping the majority of the N atoms are not electrically active but do not seem to form distinct second phases. Furthermore they do not appear to affect the basic stoichiometry or crystal structure of the CIGS. Therefore they are probably not incorporated directly into the CIGS. Apparently only the electrically-active N atoms are truly incorporated into the CIGS. Further studies may provide better methods to introduce N into CIGS to obtain high doping with low N contents. The resulting material represents a potentially interesting contact material for CIGS devices but probably not for CdTe devices as the resulting contacts were generally unsatisfactory. This was apparently due to the low work function of CIGS. It is possible that a nitrogen doped copper indium disulfide compound would produce a superior contact to CdTe but such doping was not achieved in this project.
2) Transition metal nitrides were explored as potential contacts to CdTe. While the materials were shown to have superior reflectivity compared to the conventional contacts and therefore to provide better light trapping, high quality contacts were not achieved. This may have been due as much to poor contacting technique as to the materials themselves, as optimization of the contact processing is clearly critical to achieving a high-quality contact. However, the nitrides tested almost certainly did not have a sufficiently high work function to produce adequate contacts to CdTe based on measurement of the electronic structure of the materials. Nonetheless, first quadrant roll over in the current voltage curves was not observed in most cases, as might have been expected with a poor back contact. Other transition metal nitrides could be explored but

we concluded that this class of materials is probably not the best choice compared to iron pyrite so additional studies were not carried out.

3) Amorphous Si: discussion at a workshop on contacts to CdTe suggested that p-type amorphous Si could potentially form an adequate contact to CdTe and provide the sort of minority carrier mirror that works well with Si devices ("HIT" contacts). This was studied but the contact performances were found to be modest and the contacts were unstable over time, probably due to migration of H from the a-Si:H into the CdTe. While some devices were reasonable as deposited, they degraded over the course of a day or two. Therefore a-Si:H was not pursued in detail as a contact.
4) Iron pyrite (FeS_2) was studied and found to produce as good or better contacts than the conventional contact materials and to yield good contacts under optimized conditions even without the addition of Cu. The results of the project have been communicated to First Solar and the results have been published and reported at the IEEE Photovoltaic Specialists Conference and published in Solar Eenrgy Materials and Solar Cells.

In addition to these results, we have demonstrated the use of scanning microwave impedance microscopy to characterize CdTe materials on a ~50 nanometer size scale and have shown how the technique can potentially be used to measure carrier concentration, local collection processes, and lifetime on the same scale.